

Electric-field control of magnetic anisotropies: applications to Kitaev spin liquids and topological spin textures

Shunsuke C. Furuya^{1,2,3,4} and Masahiro Sato^{1,5}

¹*Department of Physics, Ibaraki University, Mito, Ibaraki 310-8512, Japan*

²*Department of Basic Science, University of Tokyo, Meguro, Tokyo 153-8902, Japan*

³*Department of Liberal Arts, Saitama Medical University, Moroyama, Saitama 350-0495, Japan*

⁴*Institute for Solid State Physics, The University of Tokyo, Kashiwa, Japan*

⁵*Department of Physics, Chiba University, Chiba 263-8522, Japan*

(Dated: March 15, 2024)

Magnetic anisotropies often originate from the spin-orbit coupling and determine magnetic ordering patterns. We develop a microscopic theory for DC electric-field controls of magnetic anisotropies in magnetic Mott insulators and discuss its applications to Kitaev materials and topological spin textures. Throughout this paper, we take a microscopic approach based on Hubbard-like lattice models, tight-binding models with on-site interactions. We derive a low-energy spin Hamiltonian from a fourth-order perturbation expansion of the Hubbard-like model. We show in the presence of a strong intra-atomic spin-orbit coupling that DC electric fields add non-Kitaev interactions such as a Dzyaloshinskii-Moriya interaction and an off-diagonal Γ' interaction to the Kitaev-Heisenberg model and can induce a topological quantum phase transition between Majorana Chern insulating phases. We also investigate the inter-atomic Rashba spin-orbit coupling and its effects on topological spin textures. DC electric fields turn out to create and annihilate magnetic skyrmions, hedgehogs, and chiral solitons. We propose several methods of creating topological spin textures with external electromagnetic fields. Our theory clarifies that the strong but feasible electric field can control Kitaev spin liquids and topological spin textures.

I. INTRODUCTION

The spin-orbit coupling (SOC) is of significance to topological electronic states of matters [1–6]. Recently, magnetic anisotropies, a direct descendent of SOC in quantum spin systems, has enjoyed renewed theoretical and experimental interests for their essential roles in topological states of magnetic materials such as topological spin textures [7, 8] and Kitaev spin liquids [9–16].

In general, the SOC violates a part of the symmetry that the system would *a priori* possess. Should the SOC be absent, the spin rotation symmetry would be independent of the spatial rotation symmetry. However, since the SOC is always present in real materials, the spatial symmetry cannot be unrelated to the spin symmetry no matter how small the SOC is in that material. Note that the SOC is a source of the magnetic anisotropy. Here, we call the magnetic anisotropy as terms in the spin Hamiltonian that break the spin rotational symmetry¹.

An important symmetry that the SOC potentially breaks is a spatial inversion symmetry. Violating the inversion symmetry, the SOC gives rise to an antisymmetric magnetic anisotropy known as the Dzyaloshinskii-Moriya interaction (DMI) [17, 18]. The competition between the DMI and ferromagnetic exchange interactions yields topological spin textures such as magnetic skyrmions [Fig. 1 (a)] [19–23], chiral solitons [Fig. 1 (b)] [24–26], and magnetic hedgehog

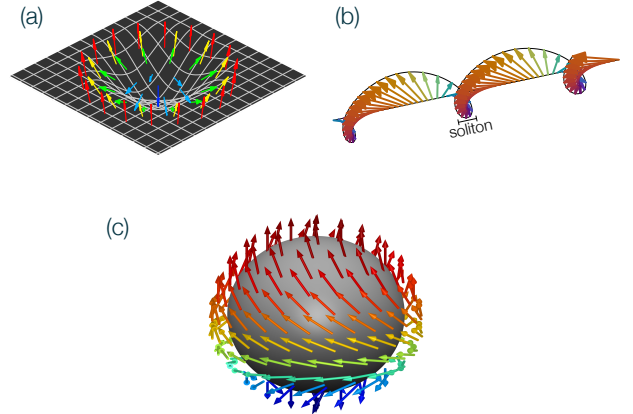


FIG. 1. Representative topological spin textures. (a) Néel-type magnetic skyrmion. (b) Chiral soliton lattice (CSL) in spin chain. (c) Magnetic hedgehog.

[Fig. 1 (c)] [27–30]. The topological spin texture carries a nonzero topological index. The nonzero topological index makes the topological spin textures robust against disturbances and prevent them from decaying into topologically trivial spin patterns such as the ferromagnetically ordered state. The topological spin texture is thus promising for device applications [7, 8, 31].

The SOC can also give rise to inversion-symmetric magnetic anisotropies such as Ising interactions (e.g., $S_i^z S_j^z$), where S_j^z denotes the z component of a localized spin S_j at the site j . This symmetric magnetic

¹ The Dzyaloshinskii-Moriya interaction and the Kitaev interaction dealt with in this paper are thus deemed magnetic anisotropies in this sense.

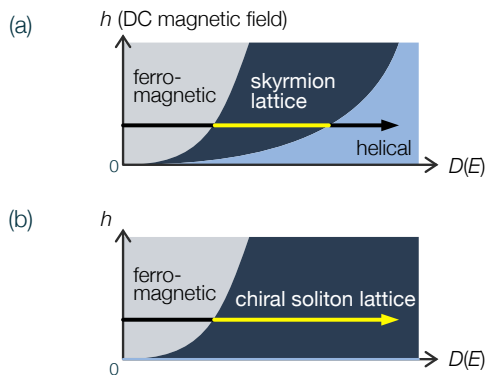


FIG. 2. (a) Schematic ground-state phase diagram of square-lattice classical Heisenberg ferromagnetic model with DMI [see Eq. (58)], including helical (HL), Skyrmion-crystal (SkX), and ferromagnetic (FM) phases [19–21, 32, 33]. The vertical axis denotes the DC magnetic field h and the horizontal axis denotes the strength of the DMI, $D(\mathbf{E})$, as a function of the DC electric field \mathbf{E} . (b) Schematic ground-state phase diagram of classical Heisenberg ferromagnetic chain with DMI [see Eq. (59)], including CSL and FM phases [24–26].

anisotropy renders the Kitaev material intriguing [10–14, 34–41]. The Kitaev material, the Kitaev model and its derivatives, has drawn intensive attraction quite some time for their significance to fundamental physics and relevance for quantum computation [10, 12, 34–40]. In light of scientific interests and engineering applications, controlling methods of these SOC-driven topological states of magnetic materials are currently one of the central issues in condensed-matter physics, quantum physics, and applied physics [42–48].

The DC electric field holds promise for external controls of topological states of magnetic materials. Historically, electric controls of magnetic systems have been discussed in the context of multiferroics [49] and spintronics [50]. For instance, noncollinear magnetic orders induce the electric polarization through a cross-correlation effect of the multiferroic material, that is, a magnetoelectric effect [49, 51–57]. For device applications, however, electric controls of the microscopic Hamiltonian is called for. Figures 2 (a) and (b) show schematic ground-state phase diagrams related to topological spin textures, which we will discuss later in Sec. IV. If we can increase the strength of the DMI $D(\mathbf{E})$ by the external electric field \mathbf{E} , we will be able to generate topological spin textures by, for example, inducing the phase transition from the ferromagnetic phase to the skyrmion-lattice phase. To discuss such interesting phase transitions, we need a microscopic theory that gives us the strength of the DMI $D(\mathbf{E})$ as a function of the DC electric field at the Hamiltonian level.

In addition, recent technological advances such as electric double-layer transistors [58, 59], ferroelectric devices [60, 61], and interfacial engineering [44, 62–64] make strong DC electric fields of $\sim 1\text{--}10$ MV/cm available.

Scanning tunneling microscopes (STMs) can also yield DC electric fields of ~ 10 MV/cm locally [65, 66]. It is natural to expect that stronger electric fields change microscopic Hamiltonian more drastically. Previously, the authors showed how the DC electric field quantitatively affects the microscopic superexchange coupling in magnetic Mott insulators [67, 68]. References [67, 68] focus on magnetically isotropic cases.

On the other hand, concerning electric-field effects on magnetically anisotropic interactions, there are many previous theoretical and experimental studies [36, 52, 53, 55, 69, 70]. However, to the best of our knowledge, no microscopic theory explicitly takes into account the geometrical configuration of ligand ions between magnetic ones to discuss electric-field effects on magnetic anisotropies. Note that most of magnetic compounds have ligand ions between magnetic ions. The ligand ion plays a crucial role in the exchange interaction between magnetic ions. Hence, it is important to develop the microscopic theory that clarifies the role of ligand ions in DC electric-field controls of magnetic anisotropies.

This paper provides the general theoretical foundation to DC electric-field controls of magnetic anisotropy in Mott insulators by explicitly taking into account the ligand ion [42–44, 50, 71–76]. Such a microscopic theory takes on a growing importance with ongoing advances in strong DC electric-field source [42, 43, 58, 59], including a single-cycle terahertz laser pulse [77–82] (see Sec. IV C). We consider two important cases: the Kitaev material and the magnetic Mott insulator with the Rashba SOC. The former has the intra-atomic SOC that defines the most relevant orbitals to the quantum magnetism. The latter has the inter-atomic SOC that will be generated on the interface of the target material to another one. Our theory clarifies that the strong but feasible electric field can control Kitaev spin liquids and topological spin textures.

This paper is organized as follows. We present a generic theoretical framework of our theory in Sec. II. We then apply our theoretical framework to two specific cases. The first case is the Kitaev spin liquid (Sec. III). The second case is topological spin textures (Sec. IV). We summarize this paper and give discussions in Sec. V.

II. FRAMEWORK

The spin Hamiltonian determining magnetic properties of Mott insulators crucially depends on virtual hopping processes of electrons under strong interactions. These hopping processes are well described by Hubbard-like tight-binding models [18, 36, 68, 70, 83–85]. Considering the locality of virtual hopping processes in the Mott insulating phase, we derive a quantum spin system from the Hubbard-like model in two stages. First, we consider a few-body electron system that contains two magnetic-ion sites (M_1 and M_2) with half-occupied d orbitals and a ligand site (L) with fully occupied p orbitals. This

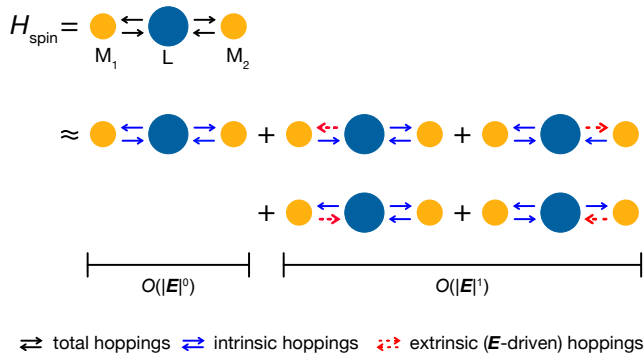


FIG. 3. Diagrammatic representation of spin Hamiltonian (3) with zeroth-order term omitted. The black solid, blue solid, and red dashed arrows denote the total hoppings $\mathcal{H}_t(\mathbf{E})$, the intrinsic hoppings $\mathcal{H}_t(\mathbf{0})$, and the \mathbf{E} -induced hoppings $\delta\mathcal{H}_t$, respectively.

three-site model contains enough ingredients to yield low-energy spin-spin interactions between two neighboring magnetic-ion sites M_1 and M_2 unless further-neighbor electron hoppings become dominant. Generally, the positional relation of the magnetic and ligand sites (such as an angle formed by M_1 , M_2 , and L) plays a critical role when determining the spin Hamiltonian under electric fields. In this paper, we focus on the isosceles triangle of Fig. 5 (b). Second, we build the many-body quantum spin model by combining many small blocks of the three-site model. In this paper, we limit ourselves to $S = 1/2$ quantum spin systems with superexchange interactions mediated by p orbitals for simplicity. Note that we can treat the $S = 1/2$ spin and a pseudospin with the spin quantum number $1/2$ on equal footings in our framework. In Sec. III, we consider a spin-orbit-entangled pseudospin, the $J_{\text{eff}} = 1/2$ doublet [36, 86–91].

This paper deals with microscopic Hubbard-like models with the following generic Hamiltonian

$$\mathcal{H} = \mathcal{H}_U(\mathbf{E}) + \mathcal{H}_t(\mathbf{E}), \quad (1)$$

where $\mathcal{H}_U(\mathbf{E})$ and $\mathcal{H}_t(\mathbf{E})$ are intra-atomic and inter-atomic terms under electric fields \mathbf{E} , respectively. Typically, the former contains on-site Coulomb repulsions and the latter does inter-atomic electron hoppings. At zero electric fields, $\mathcal{H}_t(\mathbf{0})$ denotes the intrinsic electron hoppings and the difference,

$$\delta\mathcal{H}_t(\mathbf{E}) := \mathcal{H}_t(\mathbf{E}) - \mathcal{H}_t(\mathbf{0}), \quad (2)$$

contains extrinsic \mathbf{E} -induced hoppings. We construct the Hubbard-like model (1) so that it effectively describes low-energy physics of the target material under DC electric fields. The field \mathbf{E} may contain both the external electric field generated by the experimental instrument and an effective field generated on the interface of another material. The detailed information of the material is encoded in operators and parameters of the model (1), as we will see in the next sections. For example, the SOC and a crystal-electric field lift the orbital degeneracy and define orbitals relevant to low-energy quantum spin systems. The model (1) contains the information of relevant orbitals through the definition of the creation and annihilation operators in the second-quantized form. The SOC also affects parameters included in the Hamiltonian (1). The SOC can generate spin-flipping electron hoppings intrinsically or otherwise extrinsically in collaboration with the DC electric field \mathbf{E} . Spin-flipping hoppings lead to magnetic anisotropies [18].

We regard hoppings $\mathcal{H}_t(\mathbf{E})$ as a perturbation to $\mathcal{H}_U(\mathbf{E})$ because we are focused on the Mott-insulating phase induced by the on-site interaction $\mathcal{H}_U(\mathbf{E})$. Performing the fourth-order perturbation expansion, we obtain the effective spin Hamiltonian [68],

$$\mathcal{H}_{\text{spin}} = P\mathcal{H}_U P + P\mathcal{H}_t \left(\frac{1}{E_g - \mathcal{H}_U} Q\mathcal{H}_t \right)^3 P, \quad (3)$$

where P is the projection operator to the Mott-insulating ground states of $\mathcal{H}_U(\mathbf{E})$ with the eigenenergy E_g and $Q = 1 - P$ is to its complementary space. The zeroth-order term $P\mathcal{H}_U(\mathbf{E})P$ is mostly irrelevant but gives the uniform Zeeman energy,

$$P\mathcal{H}_U P = - \sum_{a=x,y,z} \sum_j h^a S_j^a, \quad (4)$$

with $\mathbf{h} = \mathbf{g}\mathbf{B}$ for the magnetic field $\mathbf{B} = \mu_0\mathbf{H}$ [68], where \mathbf{g} is the electron's g tensor. Hereafter, we call \mathbf{h} the magnetic field for simplicity. S_j^a is the a component of the spin or pseudospin operator $\mathbf{S}_j = (S_j^x, S_j^y, S_j^z)$ for $a = x, y, z$. For details about the pseudospin, refer to Appendix A. The second term of Eq. (3) gives the ligand-mediated superexchange interaction.

The perturbation $\mathcal{H}_t(\mathbf{E})$ contains the $O(|\mathbf{E}|^0)$ term $\mathcal{H}_t(\mathbf{0})$ and the $O(|\mathbf{E}|)$ term $\delta\mathcal{H}_t(\mathbf{E})$. It is reasonable to assume that the coupling constants in $\delta\mathcal{H}_t(\mathbf{E})$ are much smaller than those in $\mathcal{H}_t(\mathbf{0})$ even under strong electric fields $\sim 1 - 10$ MV/cm [68]. Hence, we approximate the effective spin Hamiltonian (3) as follows.

$$\begin{aligned} \mathcal{H}_{\text{spin}} \approx & P\mathcal{H}_U P + P\mathcal{H}_t(\mathbf{0}) \left(\frac{1}{E_g - \mathcal{H}_U} Q\mathcal{H}_t(\mathbf{0}) \right)^3 P \\ & + P\delta\mathcal{H}_t(\mathbf{E}) \left(\frac{1}{E_g - \mathcal{H}_U} Q\mathcal{H}_t(\mathbf{0}) \right)^3 P + P\mathcal{H}_t(\mathbf{0}) \frac{1}{E_g - \mathcal{H}_U} Q\delta\mathcal{H}_t(\mathbf{E}) \left(\frac{1}{E_g - \mathcal{H}_U} Q\mathcal{H}_t(\mathbf{0}) \right)^2 P \end{aligned}$$

$$\begin{aligned}
& + P\mathcal{H}_t(\mathbf{0})\frac{1}{E_g - \mathcal{H}_U}Q\mathcal{H}_t(\mathbf{0})\frac{1}{E_g - \mathcal{H}_U}Q\delta\mathcal{H}_t(\mathbf{E})\frac{1}{E_g - \mathcal{H}_U}Q\mathcal{H}_t(\mathbf{0})P \\
& + P\mathcal{H}_t(\mathbf{0})\left(\frac{1}{E_g - \mathcal{H}_U}Q\mathcal{H}_t(\mathbf{0})\right)^2\frac{1}{E_g - \mathcal{H}_U}Q\delta\mathcal{H}_t(\mathbf{E})P.
\end{aligned} \tag{5}$$

The first term of Eq. (5) represents the zeroth-order term (4) of $\mathcal{H}_t(\mathbf{E})$ and the other terms represent fourth-order terms of $\mathcal{H}_t(\mathbf{E})$. Each fourth-order term contains one $\delta\mathcal{H}_t(\mathbf{E})$ at most since $\delta\mathcal{H}_t(\mathbf{E})$ is proportional to $|\mathbf{E}|$.

Figure 3 shows a diagrammatic representation of these fourth-order processes in Eq. (5). The black, blue, and red arrows represent the total hoppings $\mathcal{H}_t(\mathbf{E})$, the intrinsic ones $\mathcal{H}_t(\mathbf{0})$, and the \mathbf{E} -induced ones, $\delta\mathcal{H}_t(\mathbf{E})$, respectively. The intrinsic $O(|\mathbf{E}|^0)$ diagram typically contains the Heisenberg superexchange interaction [68, 83]. Hopping amplitudes of the \mathbf{E} -induced hoppings are $O(|\mathbf{E}|)$ because they arise from a distortion of electron orbitals' wave functions. Note that our generic formalism deals with such distortions of wave functions in non-magnetic ions as well as magnetic ones, as we will see later (e.g., see Sec. III C). Importantly, the electric field can break a reflection symmetry. We may rephrase the reflection-symmetry-breaking distortion as a locally generated \mathbf{E} -driven electric polarization. The atomic-scale electric polarization triggers intrinsically forbidden hopping processes $\delta\mathcal{H}_t(\mathbf{E})$. We obtain the $O(|\mathbf{E}|)$ correction to the spin Hamiltonian following the diagram.

The typical $O(|\mathbf{E}|)$ correction to the spin Hamiltonian is the DMI that breaks the inversion symmetry. The \mathbf{E} -induced DMI has been discussed in various contexts such as multiferroics [49, 51–57]. If the DMI is absent under zero electric fields, the coupling constant $\mathbf{D}(\mathbf{E})$ of the \mathbf{E} -induced DMI $\mathbf{D}(\mathbf{E}) \cdot \mathbf{S}_i \times \mathbf{S}_j$ shows the following field dependence $D^a(\mathbf{E}) \approx g^{ab}E^b + \dots$ with constant coefficients g^{ab} for $a, b = x, y, z$. Among many theoretical studies of the electric-field induction of magnetic interactions including the DMI, some studies adopt phenomenological symmetry arguments without deeply going into microscopic details [53, 55, 69] and some others adopt second-order perturbation theory similar to ours [36, 52, 70]. As we briefly mentioned in Sec. I, this paper adopts the fourth-order perturbation theory that explicitly takes into account the ligand ion and electron hoppings from and to the ligand site. The explicit inclusion of the ligand site is the most characteristic point of this paper and makes it possible to clarify the microscopic origin of the coefficients g^{ab} of the \mathbf{E} -induced DMI (see e.g., Eq (34)). Besides, our argument is not limited to the DMI but also applicable to many other magnetic anisotropies. We will show that the electric field can also yield the Γ' interaction (see e.g., Eq. (40)).

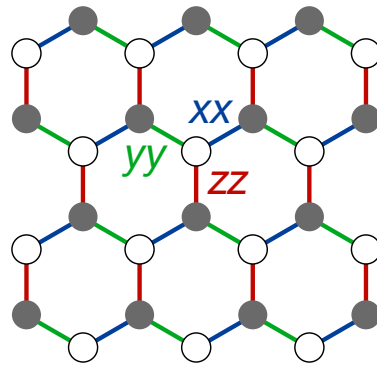


FIG. 4. Kitaev interaction on honeycomb lattice. The blue (xx), green (yy), and red (zz) bonds denote the $\langle i, j \rangle_a$ bond in Eq. (6) for $a = x, y, z$, respectively.

III. KITAEV-HEISENBERG MODEL

A. Introduction

This section is devoted to the application of the generic theory to Kitaev materials [10–12]. The Kitaev model is an $S = 1/2$ quantum spin system on the honeycomb lattice with the Hamiltonian

$$\mathcal{H}_K = \sum_{a=x,y,z} K^a \sum_{\langle i, j \rangle_a} S_i^a S_j^a, \tag{6}$$

where $\langle i, j \rangle_a$ for $a = x, y, z$ denotes the aa bond depicted in Fig. 4. S_j^a denotes the a component of the $S = 1/2$ spin operator \mathbf{S}_j at the j th site. The Hamiltonian (6) contains the Ising interaction $K^a S_i^a S_j^a$ whose direction depends on the bond $\langle i, j \rangle_a$. The Kitaev model (6) has drawn much attention in the last decade for two reasons. First, its ground state is exactly available and a spin liquid [9]. Second, Jackeli and Khaliulin showed possible realizations of the Kitaev model in spin-orbit-coupled Mott insulators [36]. Real materials have spin-spin interactions other than the Kitaev interactions (e.g., the Heisenberg interaction) however small they are. There is a family of materials whose spin Hamiltonian contains the dominant Kitaev interaction and other subleading spin-spin interactions. We call this family Kitaev materials in this paper. For instance, the Kitaev-Heisenberg model

$$\mathcal{H}_{KH} = \mathcal{H}_K + J \sum_{\langle i, j \rangle} \mathbf{S}_i \cdot \mathbf{S}_j, \tag{7}$$

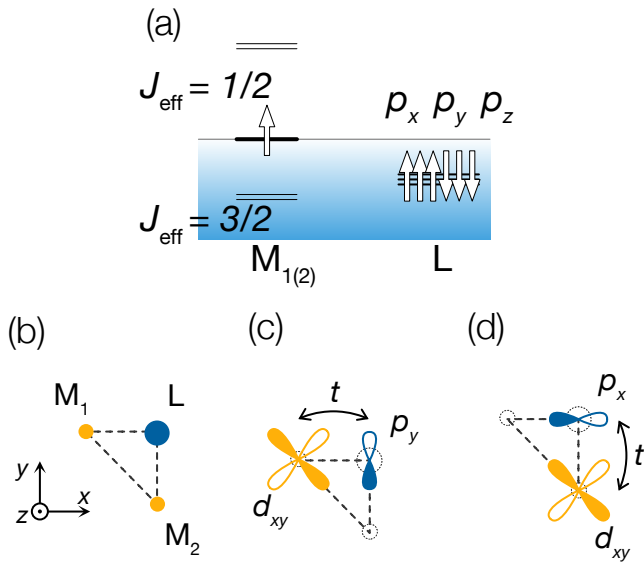


FIG. 5. (a) $J_{\text{eff}} = 1/2$ model's electron configurations in Γ_{7+} orbitals and $p_{x,y,z}$ orbitals at M_j and L sites ($j = 1, 2$). The $J_{\text{eff}} = 1/2$ orbital is half occupied while the $J_{\text{eff}} = 3/2$ orbitals at the M_j sites and the p orbitals at the L site are fully occupied. (b) Geometrical configuration of three sites, $M_{1,2}$ and L . $\Delta M_1 L M_2$ forms a right-angle isosceles triangle. (c) Electron hopping between d_{xy} orbital at M_1 and p_y orbital at L . (d) Electron hopping between d_{xy} orbital at M_2 and p_x orbital at L . The hopping between d_{xy} at M_1 (M_2) and p_x (p_y) orbital at L is forbidden by symmetries.

has often been discussed as a representative model of the Kitaev material, which may be more realistic than the Kitaev model (6). We can consider many other variants such as the Kitaev-Heisenberg- Γ' model,

$$\mathcal{H}_{\text{KH}\Gamma'} = \mathcal{H}_{\text{KH}} + \Gamma' \sum_{a=x,y,z} \sum_{b,c \neq a} \sum_{\langle i,j \rangle_a} (S_i^b S_j^c + S_i^c S_j^b), \quad (8)$$

which we discuss later in this section. This paper also deals with a variant of the Kitaev model that contains the electric-field-induced DMI.

In the rest of this section, we derive the Kitaev-Heisenberg model in the absence of the electric field and discuss how the electric field changes the model by adding extra spin-spin interactions. We show that the electric field can yield the Γ' interaction $\Gamma'(S_i^a S_j^b + S_i^b S_j^a)$ and the DMI.

B. Without electric fields

1. Few-body system

Based on the generic framework, we discuss Kitaev materials. Here, we focus on a low-spin d^5 electron configuration under the octahedral crystal electric field and the

strong SOC [36], where the $J_{\text{eff}} = 1/2$ doublet hosts a spin-orbit-entangled (pseudo)spin [Fig. 5 (a)]. The $J_{\text{eff}}^z = 1/2$ state is a superposition of t_{2g} states, $|\uparrow, l^z = 0\rangle = |d_{xy, \uparrow}\rangle$ and $|\downarrow, l^z = \pm 1\rangle = (|d_{zx, \downarrow}\rangle \pm i |d_{yz, \downarrow}\rangle)/\sqrt{2}$ [36, 86–91]. Let us denote the $J_{\text{eff}}^z = \pm 1/2$ state on the j th magnetic ion as $|\pm\rangle_j$. These pseudospin-1/2 states are written as

$$|+\rangle_j = \frac{1}{\sqrt{3}}(|d_{j,xy,\uparrow}\rangle + |d_{j,yz,\downarrow}\rangle + i |d_{j,zx,\downarrow}\rangle), \quad (9)$$

$$|-\rangle_j = \frac{1}{\sqrt{3}}(|d_{j,xy,\downarrow}\rangle - |d_{j,yz,\uparrow}\rangle + i |d_{j,zx,\uparrow}\rangle). \quad (10)$$

We consider an electric configuration shown in Fig. 5 (a). One of $|\pm\rangle_j$ is occupied on the M_j site and all the p orbitals are occupied in the L site.

Let us consider a situation where the two magnetic ions M_1 and M_2 and the one nonmagnetic ion L ² form an isosceles right triangle $\Delta M_1 L M_2$ on the xy plane [Fig. 5 (b)]. Figures 5 (c) and (d) show examples of possible hoppings between p and d orbitals. The $J_{\text{eff}} = 1/2$ doublet is the superposition of t_{2g} orbitals, as Eqs. (9) and (10) show. We first consider electron hoppings between p and t_{2g} orbitals and then rewrite the hoppings in terms of the $J_{\text{eff}} = 1/2$ doublet by projecting the t_{2g} orbitals to the doublet.

It is straightforward to write the intrinsic hoppings $\mathcal{H}_t(\mathbf{0})$ in terms of t_{2g} -orbital operators. As Figs. 5 (c) and (d) show, the electron in the p_y orbital can hop directly to the d_{xy} orbital at M_1 but cannot hop directly to that at M_2 because the d_{xy} orbital has the odd parity about a reflection $(x, y, z) \rightarrow (x, -y, z)$ but the p_y orbital has the even parity. Likewise, the electron in the p_x orbital can hop directly to the d_{xy} orbital at M_2 but cannot to that at M_1 because of the difference in the parity about another reflection $(x, y, z) \rightarrow (-x, y, z)$. Such crystalline symmetries permit the following intrinsic hoppings at $\mathbf{E} = \mathbf{0}$:

$$\mathcal{H}_t(\mathbf{0}) = t \sum_{\sigma=\pm} (p_{y,\sigma}^\dagger d_{1,xy,\sigma} + p_{z,\sigma}^\dagger d_{1,zx,\sigma} + p_{x,\sigma}^\dagger d_{2,xy,\sigma} + p_{z,\sigma}^\dagger d_{2,zx,\sigma} + \text{H.c.}). \quad (11)$$

The hopping amplitude t represents a matrix element of a single-electron Hamiltonian,

$$H_1 = \frac{\mathbf{p}^2}{2m} + V(\mathbf{x}), \quad (12)$$

where $V(x)$ is the potential that the electron feels, typically, a crystalline electric field. For example, the hopping amplitude t is given by

$$t = \langle p_{y,\sigma} | H_1 | d_{1,xy,\sigma} \rangle. \quad (13)$$

² Let us make a brief comment on the term “ion” in our context. Generally speaking, none of the M_1 , M_2 , or L sites needs to be ions. Practically, however, they are often ions that can release or receive electrons as assumed in the generic framework of Sec. II. Even though they could be other than ions, we call those sites are referred to as “ions” in this paper for notational simplicity.

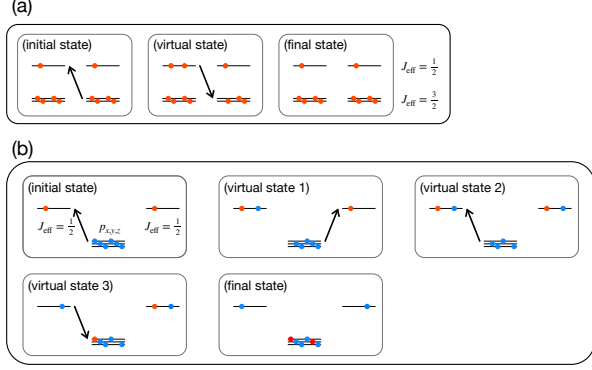


FIG. 6. (a) Second-order process to yield Kitaev model discussed in Refs. [36, 41, 91]. (b) Fourth-order process to yield Kitaev-Heisenberg model discussed in this paper. The arrows depict electron hoppings between proximate orbitals.

Note that t is independent of the index σ because H_1 of Eq. (12) has no σ dependence. In this section, we only consider the intra-atomic SOC and do not include any SOC in H_1 . When H_1 is independent of the electron spin σ , t is independent of σ . Other spatial symmetries of the triangle $\Delta M_1 L M_2$ also removes the orbital dependence of t in Eq. (11).

The $J_{\text{eff}} = 1/2$ doublet [Eqs. (9) and (10)] is the superposition of d_{xy} , d_{yz} , and d_{zx} orbitals. If we discard the d orbitals other than the $J_{\text{eff}} = 1/2$ one, we can rewrite creation and annihilations operators of those d orbitals are replaceable by those of $J_{\text{eff}} = 1/2$ ones $d_{j,\Gamma_{7+},\sigma}^\dagger$ and $d_{j,\Gamma_{7+},\sigma}$ (see Appendix A 1):

$$\mathcal{H}_t(\mathbf{0}) = \frac{t}{\sqrt{3}} \sum_{\sigma=\pm} [(p_{y,\sigma}^\dagger + ip_{z,-\sigma}^\dagger)d_{1,\Gamma_{7+},\sigma} + (p_{x,\sigma}^\dagger + \sigma p_{y,-\sigma}^\dagger)d_{2,\Gamma_{7+},\sigma} + \text{H.c.}] \quad (14)$$

Here, Γ_{7+} labels the irreducible representation of the $J_{\text{eff}} = 1/2$ doublet [86, 88].

We are now ready to write down the full Hamiltonian

$$\mathcal{H} = \mathcal{H}_U + \mathcal{H}_t(\mathbf{0}), \quad (15)$$

of the this three-site model at zero electric fields. The intrinsic hoppings and the intra-atomic interactions \mathcal{H}_U are given by Eq. (14) and

$$\begin{aligned} \mathcal{H}_U = & U_d \sum_{j=1,2} n_{j,\Gamma_{7+},+} n_{j,\Gamma_{7+},-} + U_p \sum_{\mu=x,y,z} n_{p_{\mu,+}} n_{p_{\mu,-}} \\ & + \sum_{j=1,2} V_j \sum_{\sigma=\pm} n_{j,\sigma} + V_p \sum_{\sigma=\pm} \sum_{\mu=x,y,z} n_{p_{\mu,\sigma}} \\ & - J_H \sum_{\mu \neq \mu'} \mathbf{s}_\mu \cdot \mathbf{s}_{\mu'} - \sum_{j=1,2} \sum_{a=x,y,z} h^a S_j^a, \end{aligned} \quad (16)$$

respectively. Here, $n_{j,\Gamma_{7+},\sigma} := d_{j,\Gamma_{7+},\sigma}^\dagger d_{j,\Gamma_{7+},\sigma}$ and $n_{p_{\mu,\sigma}} := p_{\mu,\sigma}^\dagger p_{\mu,\sigma}$ are the electron number operators in the $J_{\text{eff}} = 1/2$ doublet at the M_j site and p_{μ} -orbital at

the L site, respectively. U_d and U_p denote the intra-band Coulomb repulsions for the d and p orbitals, V_j and V_p are the on-site potentials at M_j and L , and $-J_H < 0$ is the ferromagnetic direct exchange between spins \mathbf{s}_μ in the p_μ orbitals.

Based on the generic framework of Fig. 3, we obtain the following spin Hamiltonian from the intrinsic hoppings (14) and the intra-atomic interactions:

$$\mathcal{H}_{\text{spin}}(\mathbf{0}) = J_F \mathbf{S}_1 \cdot \mathbf{S}_2 + K S_1^z S_2^z - \sum_{a=x,y,z} \sum_{j=1,2} h^a S_j^a \quad (17)$$

with the exchange coupling,

$$J_F = -\frac{8}{3} t^4 \left(\frac{1}{U_d - U_p + \Delta_{dp}} \right)^2 \frac{1}{2(U_d - U_p + \Delta_{dp}) - J_H}, \quad (18)$$

and the antiferromagnetic Kitaev coupling $K = -2J_F > 0$. Here, \mathbf{S}_j is the $J_{\text{eff}} = 1/2$ pseudospin (see Appendix A for its definition) and $\Delta_{dp} = E_d - E_p$ is the difference of $J_{\text{eff}} = 1/2$ -orbital eigenenergy (E_d) and the p -orbital one (E_p). The coupling J_F is not necessarily ferromagnetic. In this paper, we use parameters that yield the ferromagnetic coupling, $J_F < 0$, which is a typical case in accordance with the Goodenough-Kanamori rule [92–94]. Note also that the Kitaev coupling K is independent of the SOC because we discarded the $J_{\text{eff}} = 3/2$ levels in the derivation of Eq. (17) [Fig. 6 (b)]. Inclusion of the $J_{\text{eff}} = 3/2$ levels improves the quantitative aspect of the model, making K depend on the SOC [95, 96]. We discarded $J_{\text{eff}} = 3/2$ orbitals in this paper to keep the model as simple as possible. By contrast, the explicit inclusion of the p orbitals in our model is essential in order to discuss the electric-field effect microscopically [68].

2. Many-body systems

We can build the Kitaev-Heisenberg model

$$\mathcal{H}_{\text{KH}} = \sum_{a=x,y,z} \sum_{\langle i,j \rangle_a} (K S_i^a S_j^a + J_F \mathbf{S}_i \cdot \mathbf{S}_j) - \sum_j \mathbf{h} \cdot \mathbf{S}_j, \quad (19)$$

on the honeycomb lattice from the spin Hamiltonian (17). Let us put two triangles $\Delta M_1 L_1 M_2$ and $\Delta M_1 L_2 M_2$ on the xy plane as shown in Fig. 7 (a). Both the two triangles lead to the spin Hamiltonian (17). The M_1 - M_2 bond in this spin Hamiltonian corresponds to the zz bond (the red bond) of Fig. 4. The other bonds $a = x, y$ are derived similarly. Let us consider the xx bond (the blue bond) of Fig. 7 (b). We consider a local $x'y'z'$ coordinate system and put triangles $\Delta M_3 L_3 M_4$ and $\Delta M_3 L_4 M_4$ on the $x'y'$ plane and derive the effective spin Hamiltonian,

$$\mathcal{H}_{\text{spin}} = P \left[K S_3^{z'} S_4^{z'} + J_F \mathbf{S}_3 \cdot \mathbf{S}_4 - \sum_{j=3,4} \mathbf{h} \cdot \mathbf{S}_j \right] P. \quad (20)$$

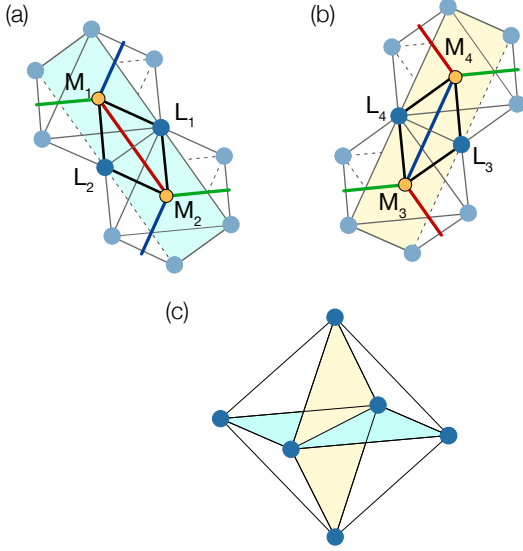


FIG. 7. (a) zz bond (red line) of Kitaev-Heisenberg model on xy plane (light blue xy plane). (b) xx bond (blue line) of Kitaev-Heisenberg model on $x'y' = yz$ plane (light yellow plane). (c) Relative positions of the two planes (a) and (b).

To combine the octahedra of Figs. 7 (a) and (b) so as to make them share an edge and form the green M_2 - M_3 bond, the xy and $x'y'z'$ coordinates should satisfy

$$(x', y', z') = (y, z, x), \quad (21)$$

turning Eq. (20) into

$$\mathcal{H}_{\text{spin}} = P \left[K S_3^x S_4^x + J_F \mathbf{S}_3 \cdot \mathbf{S}_4 - \sum_{j=3,4} \mathbf{h} \cdot \mathbf{S}_j \right] P. \quad (22)$$

In fact, we can easily confirm the relation (21) by overlapping the xy and $x'y'$ planes with a single octahedron [Fig. 7 (c)]. Repeating the same procedure, we obtain the Kitaev-Heisenberg model (19) on the honeycomb lattice of Fig. 4 We may regard that the honeycomb lattice is put on the (111) plane [36].

C. With in-plane electric fields

We go back to the three-site model on the xy plane (i.e., $z = 0$) and now give our attention to \mathbf{E} -induced interactions that are to be added to the spin Hamiltonian (17). Let us apply the in-plane electric field $\mathbf{E} = E^x \mathbf{e}_x + E^y \mathbf{e}_y$ to our three-site model on $\triangle M_1 L M_2$. The in-plane electric field breaks the reflection symmetry $(x, y, z) \rightarrow (y, x, z)$ about the $x = y$ plane. The other reflection symmetry $(x, y, z) \rightarrow (x, y, -z)$ about the $z = 0$ plane remains intact. The in-plane electric field permits hoppings that were intrinsically forbidden. Lowering the spatial symmetry of the system, the in-plane DC electric

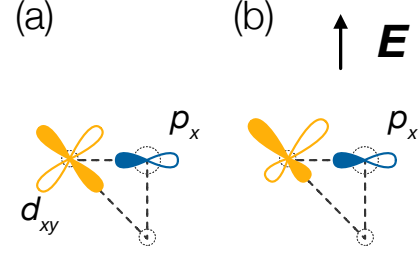


FIG. 8. (a) Proximate d_{xy} and p_x orbitals with zero overlap integral. (b) d_{xy} orbital distorted by electric field \mathbf{E} along the vertical direction. This distortion makes the overlap of the two proximate orbitals nonzero, yielding the \mathbf{E} -induced hopping $\delta\mathcal{H}_t(\mathbf{E})$.

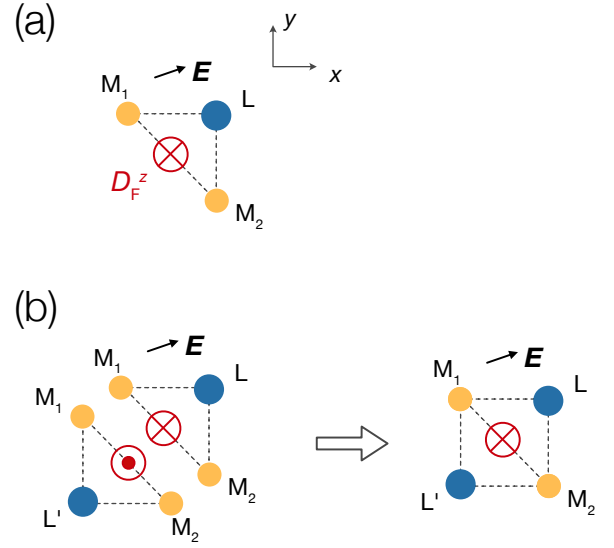


FIG. 9. (a) Out-of-plane DMI in $J_{\text{eff}} = 1/2$ model induced by in-plane \mathbf{E} . (b) Combining two triangles $\triangle M_1 L M_2$ and $\triangle M_1 L' M_2$ into a rectangle $M_1 L M_2 L'$, we obtain the DMI $D_F^z \mathbf{e}_z$ and $D_F'^z \mathbf{e}_z$, respectively. The resultant DMI on the M_1 - M_2 bond of the rectangle is $(D_F^z + D_F'^z) \mathbf{e}_z$. If L and L' are equivalent, $D_F'^z = -D_F^z$ follows from the reflection $M_1 \leftrightarrow M_2$ about the $x = y$ plane.

field induces the following hoppings between p orbitals and t_{2g} orbitals,

$$\begin{aligned} \delta\mathcal{H}_t(\mathbf{E}) = & -I \sum_{\sigma=\pm} [E^y (p_{z,\sigma}^\dagger d_{1,yz,\sigma} + p_{x,\sigma}^\dagger d_{1,xy,\sigma}) \\ & + E^x (p_{z,\sigma}^\dagger d_{2,yz,\sigma} + p_{y,\sigma}^\dagger d_{2,xy,\sigma}) + \text{H.c.}], \end{aligned} \quad (23)$$

where $-IE^y$ is the matrix element of the $-E^y P^y$ term in the single-electron Hamiltonian:

$$\begin{aligned} -IE^y &= \langle p_{x,\sigma} | (-E^y P^y) | d_{1,xy,\sigma} \rangle \\ &= -eE^y \int d\mathbf{r} \langle p_{x,\sigma} | \mathbf{r} \rangle y \langle \mathbf{r} | d_{j,xy,\sigma} \rangle. \end{aligned} \quad (24)$$

The matrix element (24) represents a reflection-symmetry-breaking distortion of the wave functions of $d_{1,xy,\sigma}$ and $p_{x,\sigma}$ orbitals caused by the electric field. The perturbation $V = -\mathbf{E} \cdot \mathbf{P}$ gives rise to the following perturbation correction to $|d_{1,xy,\sigma}\rangle$:

$$|d_{1,xy,\sigma}\rangle \rightarrow |d_{1,xy,\sigma}\rangle - \frac{\langle p_{x,\sigma} | V | d_{1,xy,\sigma} \rangle}{E_p - E_d} |p_{x,\sigma}\rangle + \dots \quad (25)$$

The similar expansion holds for $|p_{x,\sigma}\rangle$. The matrix element $\langle p_{x,\sigma} | V | d_{1,xy,\sigma} \rangle = -IE^y$ gives a measure of how much the proximate d_{xy} and p_x orbitals mix with each other. Their mixture results in the distortion of orbital probability clouds along the direction of \mathbf{E} [from Fig. 8 (a) to Fig. 8 (b)]. The distortion of the orbitals affects the spin Hamiltonian as the addition of the \mathbf{E} -induced hoppings $\delta\mathcal{H}_t(\mathbf{E})$. The additional hoppings keep the reflection symmetry about the $z = 0$ plane in accordance with the direction of the in-plane electric field. This reflection symmetry permits the DMI with the nonzero z component and with zero x and y components [Fig. 9 (a)].

To derive the \mathbf{E} -induced DMI, we first rewrite the hoppings $\delta\mathcal{H}_t(\mathbf{E})$ similarly to the intrinsic hoppings $\mathcal{H}_t(\mathbf{0})$:

$$\begin{aligned} \delta\mathcal{H}_t(\mathbf{E}) &= -\frac{I}{\sqrt{3}} \sum_{\sigma=\pm} [E^y (\sigma p_{z,-\sigma}^\dagger + p_{x,\sigma}^\dagger) d_{1,\Gamma_{7+},\sigma} \\ &\quad + E^x (\sigma p_{z,-\sigma}^\dagger + p_{y,\sigma}^\dagger) d_{2,\Gamma_{7+},\sigma} \\ &\quad + \text{H.c.}], \end{aligned} \quad (26)$$

where spin-dependent hoppings (e.g., $p_{z,-\sigma}^\dagger d_{1,\Gamma_{7+},\sigma}$) emerged because the $J_{\text{eff}} = 1/2$ doublet (9) and (10) contain spin-up and spin-down states of t_{2g} orbitals. For example, $|+\rangle_j$ contains $|d_{j,xy,\uparrow}\rangle$ and $|d_{j,zx,\downarrow}\rangle$. Straightforward calculations of Eq. (5) show that the in-plane electric field adds the following DMI

$$\mathbf{D}_F \cdot \mathbf{S}_1 \times \mathbf{S}_2 = D_F^z (\mathbf{S}_1 \times \mathbf{S}_2)^z, \quad (27)$$

with

$$\frac{D_F^z}{J_F} = -\frac{4I}{t} \frac{(E^x + E^y)(U_d - U_p + \Delta_{dp}) + (E^x - E^y)J_H}{2(U_d - U_p) + J_H}, \quad (28)$$

to the Kitaev-Heisenberg Hamiltonian (17), which is in accordance with the reflection symmetry $(x, y, z) \rightarrow (x, y, -z)$ that the in-plane electric field respects. As we did in the previous subsection, we combine $\triangle M_1 L M_2$ and $\triangle M_1 L' M_2$ into the rectangle $M_1 L M_2 L'$ [Fig. 9 (b)]. Let us suppose that the DMI generated by the in-plane \mathbf{E}

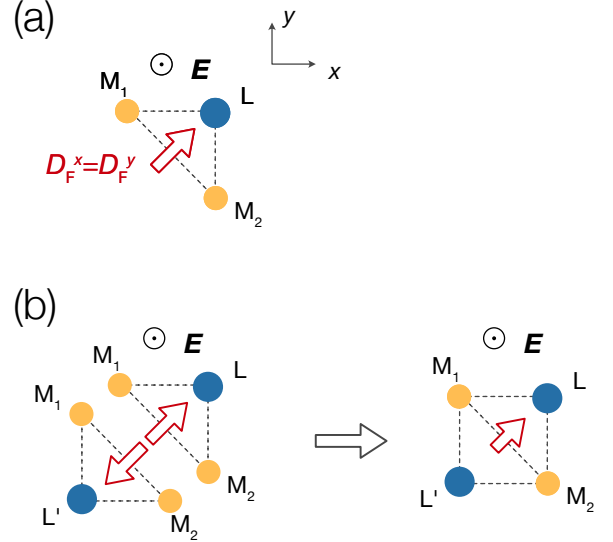


FIG. 10. (a) In-plane DMI in $J_{\text{eff}} = 1/2$ model induced by out-of-plane \mathbf{E} . The DMI has the DM vector $D_F^x \mathbf{e}_x + D_F^y \mathbf{e}_y$ with $D_F^x = D_F^y =: D_F^{\parallel}$. (b) Combining two triangles $\triangle M_1 L M_2$ and $\triangle M_1 L' M_2$ into a rectangle $M_1 L M_2 L'$, we obtain the DMI $D_F^{\parallel} (\mathbf{e}_x + \mathbf{e}_y)$ and $D_F^{\parallel} (\mathbf{e}_x + \mathbf{e}_y)$, respectively. The resultant DMI on the M_1 - M_2 bond of the rectangle is $(D_F^{\parallel} + D_F^{\parallel}) (\mathbf{e}_x + \mathbf{e}_y)$. If L and L' are equivalent, $D_F^{\parallel} = -D_F^{\parallel}$ follows from the reflection $M_1 \leftrightarrow M_2$ about the $x = y$ plane.

on these triangles are $D_F^z (\mathbf{S}_1 \times \mathbf{S}_2)^z$ and $D_F^z (\mathbf{S}_1 \times \mathbf{S}_2)^z$ as shown in Fig. 9 (b). The DMI on the M_1 - M_2 bond on the rectangle $M_1 L M_2 L'$ is their superposition, $(D_F^z + D_F^z) (\mathbf{S}_1 \times \mathbf{S}_2)^z$. Note that if L and L' are completely equivalent, $D_F^z = -D_F^z$ follows from the equivalence. The DMI is then absent in the rectangle and eventually in the honeycomb lattice (Fig. 4). The DM vector \mathbf{D}_F of the \mathbf{E} -induced DMI (27) is perpendicular to $\triangle M_1 L M_2$. Note that this direction of the DM vector perfectly accords with Moriya's symmetry argument [18] about the direction of the DM vector. The in-plane electric field keeps the inversion symmetry about the xy plane: $(x, y, z) \rightarrow (x, y, -z)$. This inversion forbids the x and y components of the DMI. Indeed, the inversion transforms the DM vector as $(D_F^x(\mathbf{E}), D_F^y(\mathbf{E}), D_F^z(\mathbf{E})) \rightarrow (-D_F^x(\mathbf{E}), -D_F^y(\mathbf{E}), D_F^z(\mathbf{E}))$, where \mathbf{E} is the in-plane electric field. The inversion symmetry about the xy plane thus leads to $D_F^x = D_F^y = 0$, in accordance with the microscopically derived result (27).

D. With out-of-plane electric fields

Let us apply an out-of-plane electric field $\mathbf{E} = E^z \mathbf{e}_z$ to the triangle $\triangle M_1 L M_2$ on the $z = 0$ plane. The out-of-plane electric field violates the reflection symmetry about the $z = 0$ plane but keeps a discrete rotational symmetry, a π -rotational one about a perpendicular bisector ℓ of

the triangle $\triangle M_1LM_2$. Note that the red-fringe arrow of Fig. 10 (a) is on the line ℓ . The line ℓ is defined as $\ell = \{(x, y, z) | y = x, z = 0\}$. The π rotation around ℓ changes $(x, y, z) \rightarrow (y, x, -z)$. Let us denote the \mathbf{E} -induced DM vector due to $\mathbf{E} = E^z \mathbf{e}_z$ as $\mathbf{D}_F(E^z)$. The π rotation $(x, y, z) \rightarrow (y, x, -z)$ affects the DMI as follows.

$$(D^x(E^z), D^y(E^z), D^z(E^z)) \rightarrow (-D^x(-E^z), -D^y(-E^z), D^z(-E^z)). \quad (29)$$

As we did in the previous subsection, we evaluate the DMI perturbatively. If we consider the linear effect of \mathbf{E} only, the DM vector is approximately an odd function of the out-of-plane field E^z : $\mathbf{D}_F(-E^z) = -\mathbf{D}_F(E^z)$. Therefore, Eq. (29) is approximated as

$$(D^x(E^z), D^y(E^z), D^z(E^z)) \rightarrow (D^x(E^z), D^y(E^z), -D^z(E^z)). \quad (30)$$

Equation (30) implies that the \mathbf{E} -induced DMI shows $D_F^x = D_F^y$ and $D_F^z = 0$ with the linear order of \mathbf{E} .

Let us derive the DMI microscopically without relying on the symmetry argument. The out-of-plane electric field induces the following hopping:

$$\begin{aligned} \delta\mathcal{H}_t(\mathbf{E}) &= -IE^z \sum_{\sigma=\pm} \sum_{j=1,2} [p_{y,\sigma}^\dagger d_{j,yz,\sigma} + p_{x,\sigma}^\dagger d_{j,zx,\sigma} + \text{H.c.}] \\ &= -\frac{IE^z}{\sqrt{3}} \sum_{\sigma,j} [(\sigma p_{y,-\sigma}^\dagger + ip_{x,-\sigma}^\dagger) d_{j,\Gamma_{7+},\sigma} + \text{H.c.}]. \end{aligned} \quad (31)$$

Repeating the same procedure as the one in the previous subsection, we straightforwardly obtain

$$\begin{aligned} \mathcal{H}_{\text{spin}} &= J_F \mathbf{S}_1 \cdot \mathbf{S}_2 + K S_1^z S_2^z - \sum_{a=x,y,z} \sum_{j=1,2} h^a S_j^a \\ &+ \mathbf{D}_F \cdot (\mathbf{S}_1 \times \mathbf{S}_2) + \Gamma' [(S_1^x + S_1^y) S_2^z + S_1^z (S_2^x + S_2^y)], \end{aligned} \quad (32)$$

with

$$\mathbf{D}_F = D_F^\parallel (\mathbf{e}_x + \mathbf{e}_y), \quad (33)$$

$$\begin{aligned} D_F^\parallel &= \frac{16t^3}{3} E^z I \left(\frac{1}{U_d - U_p + \Delta_{dp}} \right)^2 \\ &\times \frac{J_H}{4(U_d - U_p + \Delta_{dp})^2 - J_H^2}, \end{aligned} \quad (34)$$

$$\begin{aligned} \Gamma' &= \frac{32t^3}{9} E^z I \left(\frac{1}{U_d - U_p + \Delta_{dp}} \right)^2 \\ &\times \frac{U_d - U_p + \Delta_{dp}}{4(U_d - U_p + \Delta_{dp})^2 - J_H^2}. \end{aligned} \quad (35)$$

The out-of-plane electric field gives the DMI and the inversion-symmetric off-diagonal magnetic anisotropy, $\Gamma'(S_1^y S_2^z + S_1^z S_2^y)$, known as the Γ' interaction [97, 98] in the context of Kitaev materials. Both the DMI and the Γ' interaction accord with the reflection symmetry about the $x = y$ plane.

When we combine two triangles $\triangle M_1LM_2$ and $\triangle M_1L'M_2$ into the rectangle $M_1LL'M_2$ in analogy with the in-plane \mathbf{E} case, we face the same cancellation of the DMI again. If L and L' are equivalent, D_{F1}^\parallel of $\triangle M_1LM_2$ and D_{F2}^\parallel of $\triangle M_1L'M_2$ have the same magnitude and the opposite sign: $D_{F1}^\parallel = -D_{F2}^\parallel$ [Fig. 10 (b)]. Hence, the M_1 - M_2 bond of the rectangle $M_1LL'M_2$ has then no DMI after all. The relation $D_{F1}^\parallel = -D_{F2}^\parallel$ directly comes from the fact that the DMI is antisymmetric under the reflection about the $x = y$ plane. By contrast, the Γ' interaction is symmetric under that reflection. Therefore, the Γ' interaction is present on the M_1 - M_2 bond of the combined rectangle.

To conclude this subsection, we note that the spin Hamiltonian (32) indeed accords with the π -rotational symmetry about the line ℓ . As Eq. (30) shows, the \mathbf{E} -induced DMI lies in the xy plane (i.e., $D_F^z = 0$) within our theoretical scheme. Note that the out-of-plane component $D_F^z(E^z)$ is not forbidden but a higher-order effect of the electric field, practically negligible. The same argument applies to the Γ' interaction. Let us consider a generic Γ' interaction:

$$\begin{aligned} \Gamma'_x(E^z)(S_1^y S_2^z + S_1^z S_2^y) + \Gamma'_y(E^z)(S_1^z S_2^x + S_1^x S_2^z) \\ + \Gamma'_z(E^z)(S_1^x S_2^y + S_1^y S_2^x). \end{aligned} \quad (36)$$

The π rotation changes

$$\begin{aligned} (\Gamma'_x(E^z), \Gamma'_y(E^z), \Gamma'_z(E^z)) \\ \rightarrow (-\Gamma'_y(-E^z), -\Gamma'_x(-E^z), \Gamma'_z(-E^z)). \end{aligned} \quad (37)$$

If we keep the $O(\mathbf{E})$ terms only, we can approximate this transformation as

$$\begin{aligned} (\Gamma'_x(E^z), \Gamma'_y(E^z), \Gamma'_z(E^z)) \\ \rightarrow (\Gamma'_y(E^z), \Gamma'_x(E^z), -\Gamma'_z(E^z)). \end{aligned} \quad (38)$$

In other words, the \mathbf{E} -induced Γ' interaction satisfies $\Gamma'_x(E^z) = \Gamma'_y(E^z)$ and $\Gamma'_z(E^z) = 0$, as the microscopically derived spin Hamiltonian (32) shows.

E. Kitaev-Heisenberg- Γ' model under [111] electric field

Recall that the honeycomb lattice of Fig. 4 is put on the (111) plane. Now we apply the electric field $\mathbf{E}_{[111]} = E_{[111]}(\mathbf{e}_x + \mathbf{e}_y + \mathbf{e}_z)/\sqrt{3}$ so that the electric field is perpendicular to the honeycomb lattice. This electric field $\mathbf{E}_{[111]}$ has both the in-plane and out-of-plane components. Within our framework (Fig. 3) that includes the \mathbf{E} -induced hopping up to the linear order of $|\mathbf{E}|$, the $\mathbf{E}_{[111]}$ -induced magnetic anisotropies are a simple superposition of those induced by the in-plane field and the out-of-plane ones. Hence, we obtain the following spin Hamiltonian,

$$\mathcal{H}_{\text{KHF}} = \sum_{a=x,y,z} \sum_{\langle i,j \rangle_a} (K S_i^a S_j^a + J_F \mathbf{S}_i \cdot \mathbf{S}_j) - \sum_j \mathbf{h} \cdot \mathbf{S}_j$$

$$+ \Gamma'(\mathbf{E}_{[111]}) \sum_{a=x,y,z} \sum_{b,c \neq a} \sum_{\langle i,j \rangle_a} (S_i^b S_j^c + S_i^c S_j^b), \quad (39)$$

where $\Gamma'(\mathbf{E}_{[111]})$ is proportional to $E_{[111]}$:

$$\Gamma' = \frac{32t^3}{9} \frac{2E_{[111]}}{\sqrt{3}} I \left(\frac{1}{U_d - U_p + \Delta_{dp}} \right)^2 \cdot \frac{U_d - U_p + \Delta_{dp}}{4(U_d - U_p + \Delta_{dp})^2 - J_H^2}. \quad (40)$$

We assumed that the ligand sites are all equivalent. As we saw in the previous subsections, the DMI induced by $\mathbf{E}_{[111]}$ is completely canceled when L and L' are equivalent in the building blocks [Figs. 7 (a) and (b)] of the honeycomb lattice (Fig. 4). When the L and L' sites are nonequivalent, the effective spin Hamiltonian (39) further acquires the DMI. The spin Hamiltonian (39) thus contains the Kitaev interaction, the Heisenberg interaction, the Zeeman energy, and the Γ' interaction. We call it a Kitaev-Heisenberg- Γ' model in this paper.

F. Gapped quantum spin liquid

Much effort is being made to investigate effects of non-Kitaev interactions on quantum spin liquid states of the pure Kitaev model in connection with Kitaev materials such as α -RuCl₃ [99–106].

Under uniform magnetic fields $\mathbf{h} = \sum_{a=x,y,z} h^a \mathbf{e}_a$, the Kitaev model can have a gapped quantum spin liquid phase with the Chern number $C = 1$ when $h^x h^y h^z \neq 0$ [34]. The Majorana fermion in that phase has a mass gap m , the third-order of the external magnetic field:

$$m \propto \frac{h^x h^y h^z}{K^2}. \quad (41)$$

We obtain the relation (41) by regarding the Zeeman energy $-\sum_j \mathbf{h} \cdot \mathbf{S}_j$ as a perturbation to the Kitaev(-Heisenberg) model. The third-order perturbation gives rise to the mass term,

$$-\tilde{h} \sum_{\{i,j,k\}} S_i^x S_j^y S_k^z, \quad (42)$$

with $\tilde{h} \propto m \propto h^x h^y h^z / K^2$. In the presence of the perturbative Γ' interaction and the Zeeman energy, we obtain the mass term (42) in the second-order process of the perturbation expansion instead of the third-order one without the electric field. For example, let us consider the M₁-M₂ bond on the xy plane. Taking the Zeeman energy $-h^z \sum_j S_j^z$ and the Γ' interaction $\Gamma' \sum_{\langle i,j \rangle_z} (S_i^x S_j^y + S_i^y S_j^x)$ on that bond as perturbations to the Kitaev-Heisenberg Hamiltonian, we obtain [97, 98]

$$\tilde{h} \propto h^z \Gamma'. \quad (43)$$

Suppose that we have no Γ' interactions in the first place (i.e., $\Gamma' = 0$ for $\mathbf{E} = \mathbf{0}$). Then, the Majorana mass $\propto |h^x E^z|$ is the second order about the external electromagnetic fields. Furthermore, the \mathbf{E} -induced Γ' interaction can induce topological phase transitions between gapped quantum spin liquids with different Chern numbers [98]. In addition to the Γ' interaction, the electric field can also induce the DMI as we saw in this section though we need nonequivalence between ligand sites. A recent study [107] pointed out that the DMI can also drive topological quantum phase transitions between gapped quantum spin liquids under magnetic fields. Therefore, the electric field turns out to be capable of inducing various topological quantum phase transitions in combination with the magnetic field.

For α -RuCl₃, we can use parameters $U_d = 2.5$ eV, $U_p = 1.5$ eV, $\Delta_{dp} = 5.5$ eV, $J_H = 0.7$ eV, and $t = 0.88$ eV [106]. These parameters give $J_F = -3$ meV. As we mentioned, our model gives antiferromagnetic $K > 0$ but can make it ferromagnetic $K < 0$ with slight modifications of the model. If we ignore the \mathbf{E} dependence of J_F as we did thus far in this paper, we find that a DC electric field 1–10 MV/cm change $|D_F^x|$ and $|\Gamma'|$ only by 10^{-4} – 10^{-3} % of J_F , which is too much underestimated. Note that the 1–10 MV/cm DC electric field can reduce J_F by 1–10 % [68]. This reduction enhances the change in the ratios $|D_F^x/J_F|$ and $|\Gamma'/J_F|$. We can further enhance the DC electric-field effect, by including Rashba-SOC-driven hoppings besides the hitherto considered intra-atomic SOC. 1–10 % change of the SOC will have large impact on the \mathbf{E} -induced DMI. This estimation within our perturbation scheme looks experimentally challenging. However, considering the fact that many multiferroic compounds show magnetoelectric effects [49], we might be optimistic about a chance to obtain larger changes in $|\Gamma'/J_F|$ and $|D_F^x/J_F|$, depending on microscopic details of compounds not taken into account in this paper.

To conclude this section, we stress the fact that the DC electric field yields the terms such as the DMI and the Γ' interaction that were forbidden from symmetry in the absence of the electric field. This emergence of the interaction is possible because the electric field lowers the spatial symmetry.

IV. RASHBA SPIN-ORBIT COUPLING

A. Introduction

We now move on to the inter-atomic SOC. The Rashba SOC will be one of the most famous forms of such SOC. We can include the Rashba SOC into the theoretical framework through the single-electron Hamiltonian [see Eq. (12)]. We can effectively regard that the single-electron Hamiltonian H_1 contains the Rashba SOC, namely

$$-\alpha_R (\boldsymbol{\sigma} \times \mathbf{p}) \cdot \mathbf{e}(\mathbf{r}), \quad (44)$$

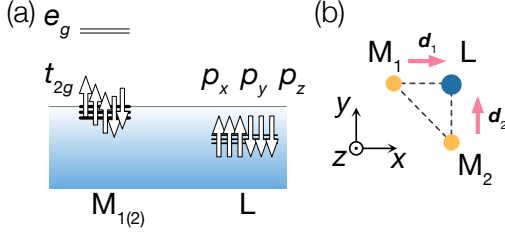


FIG. 11. (a) d^5 electron configuration of d orbitals under octahedral crystal electric field and p orbitals. (b) Spatial configuration of magnetic ions $M_{1,2}$ and ligand ion L . The red arrows depict the unit vectors \mathbf{d}_j for $j = 1, 2$ in Eq. (49). We emphasize that the intra-atomic SOC is not considered here in contrast to the setup of Fig. 5. We include the inter-atomic Rashba SOC (44).

where \mathbf{p} is the momentum of the electron in the crystal and $\mathbf{e}(\mathbf{r}) = \mathbf{E}(\mathbf{r})/|\mathbf{E}(\mathbf{r})|$ is the unit vector parallel to the electric field $\mathbf{E}(\mathbf{r})$. We can deem $\mathbf{E}(\mathbf{r})$ the external electric field, a surface electric field for thin-film materials [108, 109], or an interfacial electric field for field-effect transistors [58, 59]. The coefficient α_R is proportional to the strength of the local electric field:

$$\alpha_R \propto |\mathbf{E}(\mathbf{r})|. \quad (45)$$

The Rashba SOC affects the single-electron Hamiltonian and gives spin-flipping hoppings and eventually into the DMI.

B. Example

For demonstration, we again consider the isosceles right triangle of Fig. 11 (b). We also inherit the electron configuration, the low-spin d^5 configuration under the octahedral crystal electric field [Fig. 11 (a)]. The only difference from the previous $J_{\text{eff}} = 1/2$ model lies in the SOC mechanism. In this section, we consider Rashba-SOC-driven hoppings but ignore the d -orbital splitting due to the intra-atomic SOC.

The Rashba SOC enters into the single-electron Hamiltonian H_1 :

$$H_1 = \frac{\mathbf{p}^2}{2m} + V(\mathbf{r}) - \alpha_R \mathbf{e}(\mathbf{r}) \cdot \boldsymbol{\sigma} \times \mathbf{p}, \quad (46)$$

where m is the mass of the electron and $V(\mathbf{r})$ is the potential that the electron feels. The single-electron Hamiltonian keeps the C_{2v} symmetry [86] in the absence of the electric and magnetic fields (i.e., $\mathbf{E}(\mathbf{r}) = \mathbf{h} = \mathbf{0}$). The last term of H_1 is nothing but the Rashba SOC. The Rashba SOC enters into the Hubbard-like model via the hopping amplitude, the matrix element of the single-electron Hamiltonian. The hopping amplitude between the p_x orbital at L and the d_a orbital at M_j is given by

$$\langle p_{x,s} | H_1 | d_{j,a,s'} \rangle. \quad (47)$$

When $\mathbf{E}(\mathbf{r}) = \mathbf{0}$, the hopping amplitude in our three-site model on the isosceles right triangle is reduced to

$$\langle p_{x,s} | H_1 | d_{j,a,s'} \rangle = t \delta_{a,xy} \delta_{j,2} \delta_{s,s'}, \quad (48)$$

with a real constant t . The Rashba SOC adds another term to the right hand side of Eq. (48). For example, $\mathbf{E}(\mathbf{r}) = E^z \mathbf{e}_z$ gives

$$\begin{aligned} \langle p_{x,s} | (-\alpha_R \mathbf{e}(\mathbf{r}) \cdot \boldsymbol{\sigma} \times \mathbf{p}) | d_{j,a,s'} \rangle \\ = -\alpha_R |\mathbf{k}| e^z (\boldsymbol{\sigma}^{ss'} \times (-i\mathbf{d}_j))^z \delta_{j,2}, \end{aligned} \quad (49)$$

where we replaced the momentum $\mathbf{p} = \mathbf{k}$ by $-i|\mathbf{k}|\mathbf{d}_j$ with the unit vector \mathbf{d}_j parallel to the M_j - L bond [Fig. 11 (b)]. \mathbf{k} is the wavevector (since we set $\hbar = 1$). The Kronecker's delta $\delta_{j,2}$ appears because the vector \mathbf{d}_j is proportional to \mathbf{e}_x for $j = 1$ and to \mathbf{e}_y for $j = 2$.

Considering an application to thin-film systems on the $z = 0$ plane, we apply an out-of-plane electric field $\mathbf{E} = E^z \mathbf{e}_z$ along the z direction [1, 2]. The Rashba SOC due to the out-of-plane electric field gives

$$\begin{aligned} \delta \mathcal{H}_t(\mathbf{E}) = \sum_{s,s'} [i\lambda p_{y,s}^\dagger (\boldsymbol{\sigma}^{ss'} \times \mathbf{d}_1)^z d_{1,xy,s'} \\ + i\lambda p_{x,\sigma}^\dagger (\boldsymbol{\sigma}^{ss'} \times \mathbf{d}_2)^z d_{2,xy,s'} + \text{H.c.}], \end{aligned} \quad (50)$$

with a unit vector \mathbf{d}_j pointing toward the ligand site from M_j . The hopping amplitude λ equals to $\alpha_R |\mathbf{k}|$. The DC electric field \mathbf{E} adds this spin-dependent hopping (50) to the intrinsic spin-independent hopping,

$$\mathcal{H}_t(\mathbf{0}) = t \sum_{\sigma} (p_{y,\sigma}^\dagger d_{1,xy,\sigma} + p_{x,\sigma}^\dagger d_{2,xy,\sigma} + \text{H.c.}). \quad (51)$$

The spin Hamiltonian (3) follows the diagram of Fig. 3. We obtain the $O(|\mathbf{E}|)$ correction to the spin Hamiltonian by replacing one of the four $\mathcal{H}_t(\mathbf{E})$ by $\delta \mathcal{H}_t(\mathbf{E})$ and the others by $\mathcal{H}_t(\mathbf{0})$. Namely, we find

$$\begin{aligned} P \mathcal{H}_t(\mathbf{E}) \left(\frac{1}{E_g - \mathcal{H}_U} Q \mathcal{H}_t(\mathbf{E}) \right)^3 P \\ \approx P \mathcal{H}_t(\mathbf{0}) \left(\frac{1}{E_g - \mathcal{H}_U} Q \mathcal{H}_t(\mathbf{0}) \right)^3 P + \left[P \delta \mathcal{H}_t(\mathbf{E}) \left(\frac{1}{E_g - \mathcal{H}_U} Q \mathcal{H}_t(\mathbf{0}) \right)^3 P + \text{H.c.} \right] \end{aligned}$$

$$+ \left[P\mathcal{H}_t(\mathbf{0}) \frac{1}{E_g - \mathcal{H}_U} Q\delta\mathcal{H}_t(\mathbf{E}) \left(\frac{1}{E_g - \mathcal{H}_U} Q\mathcal{H}_t(\mathbf{0}) \right)^2 P + \text{H.c.} \right]. \quad (52)$$

The spin Hamiltonian for $\mathbf{E} = \mathbf{0}$ contains neither magnetically anisotropic terms nor inversion-asymmetric terms because the Hamiltonian $\mathcal{H}_t(\mathbf{0}) + \mathcal{H}_U$ for $\mathbf{E} = \mathbf{0}$ is magnetically isotropic and inversion symmetric. The Rashba interaction (44) breaks those spin and spatial symmetries at the same time.

Let us show results of the fourth-order perturbation expansion and give detailed derivations in Appendix B. The superexchange interaction is again ferromagnetic: $\mathcal{H}_{\text{spin}}(\mathbf{0}) = J_{\text{R}}\mathbf{S}_1 \cdot \mathbf{S}_2$ with [68]

$$J_{\text{R}} = -8t^2 \frac{J_{\text{H}}}{4(U_d - U_p + \Delta_{dp})^2 - J_{\text{H}}^2} \left(\frac{1}{U_d - U_p + \Delta_{dp}} \right)^2. \quad (53)$$

The \mathbf{E} -induced hoppings (50) yield the in-plane DMI:

$$\mathcal{H}_{\text{spin}}(\mathbf{E}) = J_{\text{R}}\mathbf{S}_1 \cdot \mathbf{S}_2 + \mathbf{D}_{\text{R}} \cdot \mathbf{S}_1 \times \mathbf{S}_2 \quad (54)$$

with

$$D_{\text{R}}^x = 32\lambda t^3 \left(\frac{1}{U_d - U_p + \Delta_{dp}} \right)^2 \frac{J_{\text{H}}}{4(U_d - U_p + \Delta_{dp})^2 - J_{\text{H}}^2}, \quad (55)$$

$$D_{\text{R}}^y = -32\lambda t^3 \left(\frac{1}{U_d - U_p + \Delta_{dp}} \right)^2 \frac{U_d - U_p + \Delta_{dp}}{4(U_d - U_p + \Delta_{dp})^2 - J_{\text{H}}^2}, \quad (56)$$

$$D_{\text{R}}^z = 0. \quad (57)$$

Note that the DMI violates the inversion symmetry about the $x = y$ plane because the Rashba SOC $-\alpha_{\text{R}}(\boldsymbol{\sigma} \times \mathbf{k})^z$ does.

For a parameter set $U_d = 3$ eV, $U_p = 2$ eV, $\Delta_{dp} = 5$ eV, $J_{\text{H}} = 1$ eV, $t = 0.1$ eV, and $\lambda = 0.05$ eV, we obtain $|D_{\text{R}}^x/J_{\text{R}}| \approx 0.46$. We used a value $\lambda = 0.05$ eV, much smaller than $\lambda = \alpha_{\text{R}}|\mathbf{k}| \propto |\mathbf{E}(\mathbf{r})|$ estimated in some materials [110, 111]. Because α_{R} is well controllable with the electric field [111], we may expect that the external DC electric field can control the DMI substantially both for Kitaev spin liquids and topological spin textures.

C. Strength of external and internal electric fields

Let us estimate the required electric-field strength. Mainly, there are two resources of the DC electric field. One is to apply it externally using, for example, field-effect transistors. The other is generated internally by crystal structures. We call the former external electric fields and the latter internal ones.

Currently, we can realize the external DC field of the strength ~ 10 MV/cm using, for example, double-layer transistors [58, 59]. The internal DC electric field can

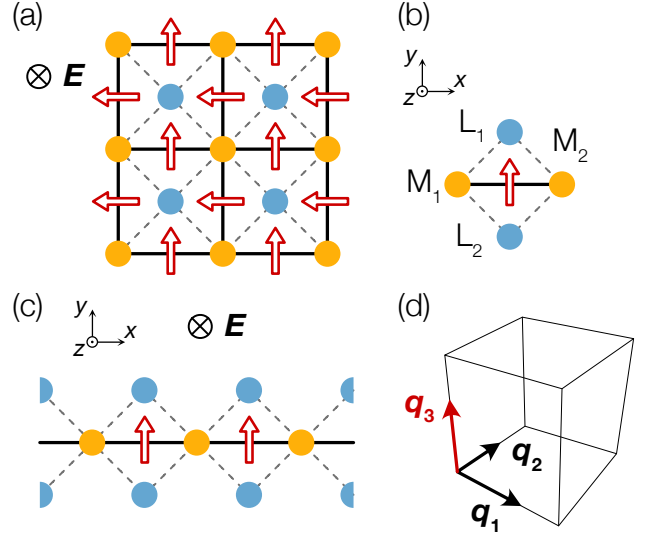


FIG. 12. (a) Edge-sharing octahedra ML_4 projected to xy plane. Magnetic ions form the square lattice (black solid lines). Intrinsic and \mathbf{E} -induced hoppings occur on dashed gray bonds. (b) Four-site model for nearest-neighbor superexchange interaction of magnetic ions. (c) One-dimensional version of square-lattice model (a), ferromagnetic spin chain with uniform DMI. (d) \mathbf{q} vectors of $3\mathbf{q}$ -hedgehog state [8, 30, 112].

be even stronger. Let us consider the octahedral crystal electric field. The strength of the crystal electric field is typically ~ 1 eV [106]. If the ligand is ~ 0.1 – 1 nm away from the magnetic ion, the internal crystal electric field is ~ 10 – 100 MV/cm. This internal crystal electric field is responsible for the Rashba SOC generated on the interface of different materials. This is the reason why the Rashba SOC can be strong, as we briefly saw in the previous subsection. We can find another interesting situation in scanning tunneling microscopes (STM) [113]. A tip of the STM induces a DC electric field strong enough to induce the tunneling electron current on the surface. If the STM tip is ~ 1 nm distant from the surface and the ~ 1 V voltage is applied, the surface feels the ~ 10 MV/cm electric field [43, 66].

A single-cycle THz laser pulse [77–82] will also be useful to generate strong DC electric fields. Though the laser pulse is not exactly static, the laser pulse can effectively be deemed a DC electric field if the time scale of the electron dynamics (~ 10 – 100 [fs]) is much faster than the duration of the applied THz laser pulse (~ 1 [ps]). The strength of the laser pulse will also reach ~ 1 MV/cm [77–80]. Here we need to be careful about the time dependence of the magnetic anisotropy induced by the THz laser pulse. The THz laser pulse can be regarded as a DC electric field when the electron hoppings

are concerned, as we mentioned above. Still, since the time scale of the spin dynamics is much slower than that of electron ones, the resultant magnetic anisotropy in the spin Hamiltonian generally shows the time dependence. The spin dynamics associated with the time-dependent spin Hamiltonian is, in principle, observable by optical measurements such as pump-probe experiments [114].

D. Applications

1. Magnetic skyrmion lattice

We can directly apply our Rashba SOC argument to controls of magnetic skyrmion lattice [19–21, 32, 33]. We exemplify this application by considering a two-dimensional (2D) array of edge-sharing octahedra whose centers have magnetic ions and vertices have ligand ions [Fig. 12 (a)]. The magnetic ions form the square lattice on the xy plane. We can build this many-body model with the small square plaquette of Fig. 12 (b) made of two isosceles right triangles $\triangle M_1 L_1 M_2$ and $\triangle M_1 L_2 M_2$. Assuming the Rashba SOC (50) on the M_j - $L_{j'}$ bonds, we obtain the spin Hamiltonian for the building block of Fig. 12 (b): $\mathcal{H}_{\text{spin}} = J_R \mathbf{S}_1 \cdot \mathbf{S}_2 + D_{\perp} \mathbf{e}_{\perp} \cdot (\mathbf{S}_1 \times \mathbf{S}_2) - h_z \sum_j S_j^z$, where we applied both the electric and magnetic fields parallel to the z axis and $\mathbf{e}_{\perp} = (\mathbf{e}_x + \mathbf{e}_y)/\sqrt{2}$ is the unit vector perpendicular to the M_1 - M_2 bond. The vector $D_{\perp} \mathbf{e}_{\perp}$ with $D_{\perp} = \sqrt{2}(D_R^x + D_R^y)$ is depicted as the red-fringe arrow in Figs. 12 (a), (b), and (c). With many square plaquettes of Fig. 12 (b), we can build a square-lattice ferromagnet [Fig. 12 (a)],

$$\begin{aligned} \mathcal{H}_{\text{SkX}} = & -|J_R| \sum_{\mathbf{r}} (\mathbf{S}_{\mathbf{r}} \cdot \mathbf{S}_{\mathbf{r}+\mathbf{e}_x} + \mathbf{S}_{\mathbf{r}} \cdot \mathbf{S}_{\mathbf{r}+\mathbf{e}_y}) - h^z \sum_{\mathbf{r}} S_{\mathbf{r}}^z \\ & + D_{\perp}(E^z) \sum_{\mathbf{r}} (\mathbf{S}_{\mathbf{r}} \times \mathbf{S}_{\mathbf{r}+\mathbf{e}_x} \cdot \mathbf{e}_y - \mathbf{S}_{\mathbf{r}} \times \mathbf{S}_{\mathbf{r}+\mathbf{e}_y} \cdot \mathbf{e}_x). \end{aligned} \quad (58)$$

The model (58) realizes the Néel-type magnetic skyrmion lattice because a 90° rotation $(S_{\mathbf{r}}^x, S_{\mathbf{r}}^y, S_{\mathbf{r}}^z) \rightarrow (-S_{\mathbf{r}}^y, S_{\mathbf{r}}^x, S_{\mathbf{r}}^z)$ turns the model (58) into the well-known model that exhibits the Bloch-type skyrmion lattice [32]. The out-of-plane electric field thus controls the ratio $D_{\perp}(E^z)/J_R(E^z)$ and allows us to create and annihilate the skyrmion. Figure 2 (a) shows the phase diagram of the model (58).

2. Chiral soliton lattice

Building the ML_2 chain [Fig. 12 (c)] with the same square plaquette, we can construct a one-dimensional version of the model (58) with the following Hamiltonian:

$$\mathcal{H}_{\text{CSL}} = -|J_R| \sum_j \mathbf{S}_j \cdot \mathbf{S}_{j+1} - h^z \sum_j S_j^z$$

$$+ D_{\perp}(E^z) \sum_j (\mathbf{e}_x \cdot \mathbf{S}_j \times \mathbf{S}_{j+1}). \quad (59)$$

The spiral order is induced by the ferromagnetic superexchange interaction and the uniform DMI along the spin chain in the x direction. The transverse magnetic field h^z perpendicular to the DMI makes the ground state the chiral soliton lattice (CSL) [25]. This ferromagnetic chain exhibits the CSL phase if it is ferromagnetically coupled to proximate spin chains in a three-dimensional crystal [26]. The ML_2 chain is typically realized for $(M, L) = (\text{Cu}, \text{O})$. The electric field controls the ratio $D_{\perp}(E^z)/J_R(E^z)$ and turns the ferromagnetic state into the CSL [Fig. 2 (b)] [24–26].

3. Magnetic hedgehog lattice

The Rashba SOC is appropriate to drive the chiral structure in a certain direction by generating a uniform DMI. This feature of the Rashba SOC will also be useful for multiple- \mathbf{q} states [Fig. 1 (c)] [8, 30, 112]. Provided that a magnetic material shows a double- \mathbf{q} state with the two \mathbf{q} vectors lying on the q_x - q_y plane [\mathbf{q}_1 and \mathbf{q}_2 of Fig. 12 (d)] and the electric field \mathbf{E} adds another \mathbf{q} vector (\mathbf{q}_3). This feature of the electric field will drive the magnetic hedgehog lattice where the triple- or quadruple- \mathbf{q} spin texture is required.

We can consider another interesting situation, where the single- \mathbf{q} state is initially realized without the electric field. Suppose the single- \mathbf{q} configuration along the z axis. The electric field can add a double- \mathbf{q} spin texture on the xy plane to the single- \mathbf{q} state, leading to the triple- \mathbf{q} state [115].

V. SUMMARY AND DISCUSSIONS

This paper provides the general theoretical foundation to DC electric-field controls of magnetic Mott insulators [42–44, 50, 71–76]. Our formalism treats the electric-field effect on electron orbitals of magnetic and nonmagnetic ions perturbatively. As Fig. 3 shows, we considered the fourth-order perturbation expansion about the hopping amplitude because we explicitly take into account the nonmagnetic ligand ion. The explicit inclusion of nonmagnetic ions is essential to incorporate the DC electric-field effect. In fact, the electric field lowers the spatial symmetry and induces electron hoppings between magnetic and nonmagnetic ions that were forbidden from the crystalline symmetry. The symmetry restricts the possible form of the spin Hamiltonian. For example, the DMI is allowed in the presence of the DC electric field even when it is forbidden in the absence of the electric field. The DM vector of such a DMI is obviously dependent on the electric field and approximately proportional to the electric field when the field is perturbative. This phenomenon of the electric-field-induced

DMI itself has been known for years. More specifically, the Rashba-SOC-induced DMI has been discussed for years [63, 64, 111, 116, 117]. What we did thus far in this paper is to derive the DMI on the microscopic basis. Note that the symmetry argument implies the induction of the magnetic anisotropy such as the DMI by the electric field but does not tell how large the induced anisotropy is. We did not rely on the symmetry argument in the derivation of the magnetic anisotropy. The microscopic derivation is important because it tells us how large the induced magnetic anisotropy is and what parameters we should tune to obtain more efficient or drastic electric-field effects.

We considered two important cases: the Kitaev material and the magnetic Mott insulator with the Rashba SOC. In the Kitaev material, we proposed that the electric field generates the DMI and the off-diagonal Γ' interaction that can potentially induce phase transitions [e.g., Eqs. (32) and (39)]. We also showed that the electric-field-induced Rashba SOC gives rise to the DMI, essential to realize topological spin textures such as the magnetic skyrmion, the CSL, and the magnetic hedgehog [e.g., Eqs. (58) and (59)]. Here, we did not discuss the intra-atomic SOC in the p orbital of the ligand ion because it will be much smaller than the two SOC dealt with in this paper.

For experiments, we propose to use (quasi-)2D systems. We can generally apply strong enough electric fields to quasi-2D materials with state-of-the-art techniques such as double-layer transistors [59] and STM [65]. The above-mentioned α -RuCl₃ [118] and other Kitaev-candidate materials such as Na₂IrO₃ [10, 36] have a quasi-2D layered honeycomb structure. Quasi-2D materials are compatible with the strong DC electric-field source [42, 43, 58, 59]. Besides, the quasi-2D structure allows us to use the strong electric field on the interface to another material. Generation of strong surface electric fields were already experimentally available [58, 59]. Reference [44] gives an experimental controlling method of the DMI with the interface electric field in the SrRuO₃-SrIrO₃ bilayer system. We point out the possible relevance of our study to 2D van der Waals magnets [16, 119, 120] since the 2D van der Waals magnets exhibit large electric-field effects. Electric-field switching between ferromagnetic and antiferromagnetic states were already experimentally reported [121, 122]. We hope that our paper will stimulate electric-field controls of magnetic *anisotropies* in those quasi-2D magnets.

ACKNOWLEDGMENTS

The authors are grateful to Tetsuo Hanaguri and Minoru Kanega for fruitful discussions. S.C.F. and M.S. are supported by a Grant-in-Aid for Scientific Research on Innovative Areas "Quantum Liquid Crystals" Grant No. JP19H05825. S.C.F. is also supported by JSPS Grants-in-Aid for Transformative Research Areas (A) "Extreme

Universe," (Grants Nos. JP21H05191 and 21H05182) and by JSPS KAKENHI (Grants Nos. JP20K03769 and JP21K03465). M.S. is also supported by JSPS KAKENHI (Grant Nos. 20H01830 and 20H01849) and by a Grant-in-Aid for Scientific Research on Innovative Areas "Evolution of Chiral Materials Science using Helical Light Fields" (Grants No. JP22H05131 and No. JP23H04576) from JSPS of Japan.

Appendix A: Field-induced magnetic anisotropies in Kitaev-Heisenberg model

1. Effective mapping from t_{2g} orbitals to $J_{\text{eff}} = 1/2$ doublet

The $J_{\text{eff}} = 1/2$ doublet at M_j are a spin-orbit-entangled superposition of t_{2g} orbitals. The up state ($|+\rangle_j$) and the down state ($|-\rangle_j$) state of the (pseudo)spin at M_j are given by [52, 87, 90, 91]

$$|+\rangle_j = \frac{1}{\sqrt{3}}(|d_{j,xy,\uparrow}\rangle + |d_{j,yz,\downarrow}\rangle + i|d_{j,zx,\downarrow}\rangle), \quad (\text{A1})$$

$$|-\rangle_j = \frac{1}{\sqrt{3}}(|d_{j,xy,\downarrow}\rangle - |d_{j,yz,\uparrow}\rangle + i|d_{j,zx,\uparrow}\rangle), \quad (\text{A2})$$

where $|d_{j,a,\sigma}\rangle = d_{j,a,\sigma}^\dagger |0\rangle$ is a spin- σ state of the d_a -orbital electron at M_j and $|0\rangle$ is the vacuum of the creation operator $d_{j,a,\sigma}^\dagger$. This doublet is labeled as Γ_{7+} using the Bethe's notation of the double group [88]. Hereafter, we denote $\sigma = \uparrow, \downarrow$ as $\sigma = +, -$, respectively. Note that under the strong spin-orbit coupling (SOC), we should adopt the so-called JJ coupling scheme instead of the LS coupling one [90, 91]. Here, \mathbf{J} is a superposition of the angular momentum \mathbf{L} and the spin \mathbf{S} [see Eq. (A4)]. Whereas the SOC enters into wave functions of hybridized orbitals in the LS -coupling scheme, it does not in the strongly spin-orbit-entangled states (A1) and (A2) in the JJ -coupling scheme. This difference comes out of a fact that the former deals with the SOC perturbatively but the latter does nonperturbatively. In Eqs. (A1) and (A2) formulated within the JJ -coupling scheme, the coefficients are fully determined by the crystalline symmetry.

The creation and annihilation operators of the t_{2g} -orbital electrons are related to each other in the $J_{\text{eff}} = 1/2$ model because the $J_{\text{eff}} = 1/2$ doublet is their superposition. Here, we note that the orbital angular momentum $\mathbf{L} = -\mathbf{l}_d$ and the spin,

$$\mathbf{S}_d := \frac{\hbar}{2} \sum_{a=xy,yz,zx} \sum_{s,s'=\pm} d_{j,a,s}^\dagger \boldsymbol{\sigma}^{ss'} d_{j,a,s'}, \quad (\text{A3})$$

form the effective total angular momentum \mathbf{J}_{eff} as follows [89].

$$\mathbf{J}_{\text{eff}} = -\mathbf{l}_d + \mathbf{S}_d. \quad (\text{A4})$$

Hereafter, we set $\hbar = 1$ for simplicity. \mathbf{S}_d and \mathbf{L} of the Γ_{7+} doublet are antiparallel to each other because electrons in the d^5 configuration feel the strong SOC $\xi \mathbf{L} \cdot \mathbf{S}_d$ with large positive ξ [89]. We can easily confirm

$$J_{\text{eff}}^z |\pm\rangle_j = \pm \frac{1}{2} |\pm\rangle_j. \quad (\text{A5})$$

Since there are few possibilities of confusions, we simply represent this pseudospin \mathbf{J}_{eff} as \mathbf{S}_j and call it a spin, as we did in the main text. The spin operator \mathbf{S}_j is thus defined as

$$S_j^z = \frac{1}{2} (|+\rangle_{jj} \langle +| - |-\rangle_{jj} \langle -|), \quad (\text{A6})$$

$$S_j^\pm = |\pm\rangle_{jj} \langle \mp|. \quad (\text{A7})$$

Our purpose in this subsection is to write the spin Hamiltonian in terms of this spin operator \mathbf{S}_j . For this purpose, we represent creation and annihilation operators of the t_{2g} orbitals in terms of the $J_{\text{eff}} = 1/2$ doublet, $d_{j,\Gamma_{7+},\sigma}^\dagger$ and $d_{j,\Gamma_{7+},\sigma}$. They are defined as

$$|+\rangle_j =: d_{j,\Gamma_{7+},+}^\dagger |0\rangle, \quad |-\rangle_j =: d_{j,\Gamma_{7+},-}^\dagger |0\rangle. \quad (\text{A8})$$

An operator, $n_{j,\Gamma_{7+},\sigma} = d_{j,\Gamma_{7+},\sigma}^\dagger d_{j,\Gamma_{7+},\sigma}$, counts the number of electrons with the σ spin in the Γ_{7+} doublet. We can relate t_{2g} -orbital operators $d_{j,a,\sigma}$ with $a = xy, yz, zx$ to the Γ_{7+} -orbital operator $d_{j,\Gamma_{7+},\sigma}$ as follows. For example, the operator $d_{j,xy,\sigma}$ satisfies

$$d_{j,xy,+} |\sigma\rangle_j = \frac{1}{\sqrt{3}} \delta_{\sigma,+} |0\rangle, \quad d_{j,xy,-} |\sigma\rangle_j = \frac{1}{\sqrt{3}} \delta_{\sigma,-} |0\rangle, \quad (\text{A9})$$

where $\delta_{a,b}$ is Kronecker's delta. These relations indicate

$$d_{j,xy,\sigma} P = Q d_{j,xy,\sigma} P = Q \left(\frac{1}{\sqrt{3}} d_{j,\sigma} \right) P, \quad (\text{A10})$$

at low energies, where $P = \bigotimes_{j=1,2} (|+\rangle_{jj} \langle +| + |-\rangle_{jj} \langle -|)$ is the projection operator to the Hilbert subspace spanned by the Γ_{7+} doublets and $Q = 1 - P$ is the projection to its complementary. Note a simple relation $P d_{j,a,\sigma} P = 0$ for $a = xy, yz, zx$. Likewise, we obtain

$$d_{j,yz,\sigma} P = Q d_{j,yz,\sigma} P = Q \left(-\frac{1}{\sqrt{3}} \sigma d_{j,-\sigma} \right) P, \quad (\text{A11})$$

$$d_{j,zx,\sigma} P = Q d_{j,zx,\sigma} P = Q \left(i \frac{1}{\sqrt{3}} d_{j,-\sigma} \right) P. \quad (\text{A12})$$

These relations lead to

$$\mathcal{H}_t(\mathbf{0})P = \left\{ \frac{t}{\sqrt{3}} \sum_{\sigma=\pm} [(p_{y,\sigma}^\dagger + ip_{z,-\sigma}^\dagger) d_{1,\Gamma_{7+},\sigma} + (p_{x,\sigma}^\dagger + \sigma p_{y,-\sigma}^\dagger) d_{2,\Gamma_{7+},\sigma} + \text{H.c.}] \right\} P, \quad (\text{A13})$$

$$P \mathcal{H}_t(\mathbf{0}) = P \left\{ \frac{t}{\sqrt{3}} \sum_{\sigma=\pm} [(p_{y,\sigma}^\dagger + ip_{z,-\sigma}^\dagger) d_{1,\Gamma_{7+},\sigma} + (p_{x,\sigma}^\dagger + \sigma p_{y,-\sigma}^\dagger) d_{2,\Gamma_{7+},\sigma} + \text{H.c.}] \right\}. \quad (\text{A14})$$

At low energies, we can abbreviate these relations as Eq. (14) in the main text.

2. Evaluation of I

To evaluate the constant I , we adopt the wave functions $\langle \mathbf{r} | d_{j,xy,\sigma} \rangle$ and $\langle \mathbf{r} | p_{xy,\sigma} \rangle$ of the hydrogen-like atom in terms of the polar coordinate $\mathbf{r} = r(\sin \theta \cos \phi, \sin \theta \sin \phi, \cos \theta)$:

$$\langle \mathbf{r} | d_{j,xy,\sigma} \rangle \approx R_{nd}(r) Y_{xy}(\theta, \phi), \quad (\text{A15})$$

$$\langle \mathbf{r} | p_{x,\sigma} \rangle \approx R_{2p}(r) Y_x(\theta, \phi), \quad (\text{A16})$$

$$R_{3d}(r) = \frac{4}{81\sqrt{30}} \left(\frac{Z_M}{a_0} \right)^{3/2} \left(\frac{Z_M r}{a_0} \right)^2 \exp\left(-\frac{Z_M r}{3a_0}\right), \quad (\text{A17})$$

$$R_{4d}(r) = \frac{1}{768\sqrt{5}} \left(\frac{Z_M}{a_0} \right)^{3/2} \left(12 - \frac{Z_M r}{a_0} \right) \left(\frac{Z_M r}{a_0} \right)^2 \times \exp\left(-\frac{Z_M r}{4a_0}\right), \quad (\text{A18})$$

$$R_{2p}(r) = \frac{1}{2\sqrt{6}} \left(\frac{Z_L}{a_0} \right)^{3/2} \frac{Z_L}{a_0} r \exp\left(-\frac{Z_L r}{2a_0}\right), \quad (\text{A19})$$

$$Y_{xy}(\theta, \phi) = \sqrt{\frac{15}{16\pi}} \sin^2 \theta \sin(2\phi), \quad (\text{A20})$$

$$Y_x(\theta, \phi) = \sqrt{\frac{3}{4\pi}} \sin \theta \cos \phi. \quad (\text{A21})$$

Here, a_0 , Z_M , and Z_L are the Bohr radius and the atomic numbers of M_j and L , respectively [52, 86]. $n = 3, 4, \dots$ represent the principal quantum number. For $n = 3$, these wave functions lead to

$$I \approx e a_0 \frac{16}{27} Z_M^{7/2} Z_L^{5/2} \left(\frac{Z_M}{3} + \frac{Z_L}{2} \right)^{-7}. \quad (\text{A22})$$

For $n = 4$, it becomes

$$I \approx e a_0 \frac{\sqrt{3}}{16} Z_M^{7/2} Z_L^{5/2} \left(\frac{Z_M}{4} + \frac{Z_L}{2} \right)^{-8}. \quad (\text{A23})$$

Appendix B: Rashba spin-orbit interaction in tight-binding models

To show that the Rashba SOC leads to the DMI, we consider the second term,

$$P\delta\mathcal{H}_t(\mathbf{E})\left(\frac{1}{E_g - \mathcal{H}_U}Q\mathcal{H}_t(\mathbf{0})\right)^3 P + \text{H.c.}, \quad (\text{B1})$$

of Eq. (52) The second line of Eq. (52) is similarly calculated. The fourth-order perturbation processes are divided into two classes, the processes (a) and (b) of FIG. 18 in Ref. [68]. The process (a) gives

$$\begin{aligned} & \left[P\delta\mathcal{H}_t(\mathbf{E})\left(\frac{1}{E_g - \mathcal{H}_U}Q\mathcal{H}_t(\mathbf{0})\right)^3 P + \text{H.c.} \right]_{\text{process (a)}} \\ &= P \left[\frac{i\lambda t}{U_d - U_p + \Delta_{dp}} \frac{t^2}{2(U_d - U_p) + 2\Delta_{dp} - J_H} \frac{2}{U_d - U_p + \Delta_{dp}} \right. \\ & \quad \cdot \left\{ \sum_{\sigma_1, \sigma_2, \dots, \sigma_5 = \pm} \frac{1}{2} \delta_{\sigma_1, -\sigma_2} (-\delta_{\sigma_4, \sigma_2} \delta_{\sigma_3, \sigma_1} - \delta_{\sigma_4, -\sigma_2} \delta_{\sigma_3, -\sigma_1}) (\boldsymbol{\sigma}_{\sigma_4 \sigma_5} \times \mathbf{d}_2)^z d_{2, \sigma_5} d_{1, \sigma_3} d_{2, \sigma_2}^\dagger d_{1, \sigma_1}^\dagger \right. \\ & \quad \left. + \sum_{\sigma_1, \sigma_2, \dots, \sigma_5} \frac{1}{2} \delta_{\sigma_1, -\sigma_2} (\delta_{\sigma_4, \sigma_2} \delta_{\sigma_3, \sigma_1} + \delta_{\sigma_4, -\sigma_2} \delta_{\sigma_3, -\sigma_1}) (\boldsymbol{\sigma}_{\sigma_4 \sigma_5} \times \mathbf{d}_1)^z d_{1, \sigma_5} d_{2, \sigma_3} d_{2, \sigma_2}^\dagger d_{1, \sigma_1}^\dagger \right\} \\ & \quad + \frac{i\lambda t}{U_d - U_p + \Delta_{dp}} \frac{t^2}{2(U_d - U_p) + 2\Delta_{dp} + J_H} \frac{2}{U_d - U_p + \Delta_{dp}} \\ & \quad \cdot \left\{ \sum_{\sigma_1, \sigma_2, \dots, \sigma_5 = \pm} \frac{1}{2} \delta_{\sigma_1, -\sigma_2} (-\delta_{\sigma_4, \sigma_2} \delta_{\sigma_3, \sigma_1} + \delta_{\sigma_4, -\sigma_2} \delta_{\sigma_3, -\sigma_1}) (\boldsymbol{\sigma}_{\sigma_4 \sigma_5} \times \mathbf{d}_2)^z d_{2, \sigma_5} d_{1, \sigma_3} d_{2, \sigma_2}^\dagger d_{1, \sigma_1}^\dagger \right. \\ & \quad \left. + \sum_{\sigma_1, \sigma_2, \dots, \sigma_5 = \pm} \frac{1}{2} \delta_{\sigma_1, -\sigma_2} (\delta_{\sigma_4, \sigma_2} \delta_{\sigma_3, \sigma_1} - \delta_{\sigma_4, -\sigma_2} \delta_{\sigma_3, -\sigma_1}) (\boldsymbol{\sigma}_{\sigma_4 \sigma_5} \times \mathbf{d}_1)^z d_{1, \sigma_5} d_{2, \sigma_3} d_{2, \sigma_2}^\dagger d_{1, \sigma_1}^\dagger \right\} \Big] P, \quad (\text{B2}) \end{aligned}$$

where we already removed the p -orbital operators by using the projection P [see, for example, Eq. (A3) of Ref. [68]]. Rewriting the d -orbital creation and annihilation operators in terms of the spin \mathbf{S}_j ($j = 1, 2$), we obtain

$$\begin{aligned} & \left[P\delta\mathcal{H}_t(\mathbf{E})\left(\frac{1}{E_g - \mathcal{H}_U}Q\mathcal{H}_t(\mathbf{0})\right)^3 P + \text{H.c.} \right]_{\text{process (a)}} \\ &= P \left[\frac{-4\lambda t^3}{2(U_d - U_p) + 2\Delta_{dp} - J_H} \left(\frac{1}{U_d - U_p + \Delta_{dp}} \right)^2 \right. \\ & \quad \cdot [d_2^y (-S_1^z S_2^y - S_1^y S_2^z) + d_2^x (-S_1^z S_2^x - S_1^x S_2^z) + d_1^y (-S_1^z S_2^y - S_1^y S_2^z) + d_1^x (-S_1^z S_2^x - S_1^x S_2^z)] \\ & \quad + \frac{-4\lambda t^3}{U_d - U_p + 2\Delta_{dp} + J_H} \left(\frac{1}{U_d - U_p + \Delta_{dp}} \right)^2 \\ & \quad \cdot [d_2^y (-S_1^z S_2^y + S_1^y S_2^z) + d_2^x (-S_1^z S_2^x + S_1^x S_2^z) + d_1^y (-S_1^z S_2^y + S_1^y S_2^z) + d_1^x (-S_1^z S_2^x + S_1^x S_2^z)] \Big] P. \quad (\text{B3}) \end{aligned}$$

The process (b) of FIG. 18 in Ref. [68] gives

$$\begin{aligned} & \left[P\delta\mathcal{H}_t(\mathbf{E})\left(\frac{1}{E_g - \mathcal{H}_U}Q\mathcal{H}_t(\mathbf{0})\right)^3 P + \text{H.c.} \right]_{\text{process (b)}} \\ &= P \left[\frac{i\lambda t}{U_d - U_p + \Delta_{dp}} \frac{t^2}{2(U_d - U_p) + 2\Delta_{dp} - J_H} \frac{2}{U_d - U_p + \Delta_{dp}} \right. \\ & \quad \cdot \sum_{\sigma_1, \dots, \sigma_5} \delta_{\sigma_1, \sigma_2} (-\delta_{\sigma_4, \sigma_2} \delta_{\sigma_3, \sigma_1}) (\boldsymbol{\sigma}_{\sigma_4 \sigma_5} \times \mathbf{d}_2)^z d_{2, \sigma_5} d_{1, \sigma_3} d_{2, \sigma_2}^\dagger d_{1, \sigma_1}^\dagger \\ & \quad + \frac{i\lambda t}{U_d - U_p + \Delta_{dp}} \frac{t^2}{2(U_d - U_p) + 2\Delta_{dp} - J_H} \frac{2}{U_d - U_p + \Delta_{dp}} \\ & \quad \cdot \sum_{\sigma_1, \dots, \sigma_5} \delta_{\sigma_1, \sigma_2} (\delta_{\sigma_4, \sigma_2} \delta_{\sigma_3, \sigma_1}) (\boldsymbol{\sigma}_{\sigma_4 \sigma_5} \times \mathbf{d}_1)^z d_{1, \sigma_5} d_{2, \sigma_3} d_{2, \sigma_2}^\dagger d_{1, \sigma_1}^\dagger \\ & \quad \left. + \text{H.c.} \right] P \end{aligned}$$

$$\begin{aligned}
&= P \left[\frac{-8\lambda t^3}{2(U_d - U_p) + 2\Delta_{dp} - J_H} \left(\frac{1}{U_d - U_p + \Delta_{dp}} \right)^2 (d_2^y S_1^z S_2^y + d_2^x S_1^z S_2^x) \right. \\
&\quad \left. + \frac{-8\lambda t^3}{2(U_d - U_p) + 2\Delta_{dp} - J_H} \left(\frac{1}{U_d - U_p + \Delta_{dp}} \right)^2 (d_1^y S_1^y S_2^z + d_1^x S_1^x S_2^z) \right] P. \tag{B4}
\end{aligned}$$

Combining these contributions of the two processes together, we obtain

$$\begin{aligned}
&P\delta\mathcal{H}_t(\mathbf{E}) \left(\frac{1}{E_g - \mathcal{H}_U} Q\mathcal{H}_t(\mathbf{0}) \right)^3 P + \text{H.c.} \\
&= P \left[\frac{-4\lambda t^3}{2(U_d - U_p) + 2\Delta_{dp} - J_H} \frac{1}{U_d - U_p + \Delta_{dp}} [(d_1^y - d_2^y)(\mathbf{S}_1 \times \mathbf{S}_2)^x - (d_1^x - d_2^x)(\mathbf{S}_1 \times \mathbf{S}_2)^y] \right. \\
&\quad \left. + \frac{-4\lambda t^3}{2(U_d - U_p) + 2\Delta_{dp} + J_H} \frac{1}{U_d - U_p + \Delta_{dp}} [(d_1^y + d_2^y)(\mathbf{S}_1 \times \mathbf{S}_2)^x - (d_1^x + d_2^x)(\mathbf{S}_1 \times \mathbf{S}_2)^y] \right] P, \tag{B5}
\end{aligned}$$

which is nothing but the DMI. The other terms,

$$P\mathcal{H}_t(\mathbf{0}) \frac{1}{E_g - \mathcal{H}_U} Q\delta\mathcal{H}_t(\mathbf{E}) \left(\frac{1}{E_g - \mathcal{H}_U} Q\mathcal{H}_t(\mathbf{0}) \right)^2 P + \text{H.c.} \tag{B6}$$

lead to the same result after repeating a similar procedure to the above one. Collecting all these contributions, we reach the final result:

$$\mathcal{H}_{\text{spin}} = J\mathbf{S}_0 \cdot \mathbf{S}_1 + D^x(\mathbf{S}_1 \times \mathbf{S}_2)^x + D^y(\mathbf{S}_1 \times \mathbf{S}_2)^y, \tag{B7}$$

$$D^x = - \left[(d_1^y - d_2^y) \frac{16\lambda t^3}{2(U_d - U_p) + 2\Delta_{dp} - J_H} + (d_1^y + d_2^y) \frac{16\lambda t^3}{2(U_d - U_p) + 2\Delta_{dp} + J_H} \right] \left(\frac{1}{U_d - U_p + \Delta_{dp}} \right)^2, \tag{B8}$$

$$D^y = \left[(d_1^x - d_2^x) \frac{16\lambda t^3}{2(U_d - U_p) + 2\Delta_{dp} - J_H} + (d_1^x + d_2^x) \frac{16\lambda t^3}{2(U_d - U_p) + 2\Delta_{dp} + J_H} \right] \left(\frac{1}{U_d - U_p + \Delta_{dp}} \right)^2. \tag{B9}$$

Note that $\mathbf{d}_1 = \mathbf{e}_x$ and $\mathbf{d}_2 = \mathbf{e}_y$ for the spatial configuration of Fig. 11 (b).

-
- [1] C. L. Kane and E. J. Mele, Z_2 Topological Order and the Quantum Spin Hall Effect, *Phys. Rev. Lett.* **95**, 146802 (2005).
 - [2] C. L. Kane and E. J. Mele, Quantum Spin Hall Effect in Graphene, *Phys. Rev. Lett.* **95**, 226801 (2005).
 - [3] C. Nayak, S. H. Simon, A. Stern, M. Freedman, and S. Das Sarma, Non-Abelian anyons and topological quantum computation, *Rev. Mod. Phys.* **80**, 1083 (2008).
 - [4] M. Z. Hasan and C. L. Kane, Colloquium: Topological insulators, *Rev. Mod. Phys.* **82**, 3045 (2010).
 - [5] X.-L. Qi and S.-C. Zhang, Topological insulators and superconductors, *Rev. Mod. Phys.* **83**, 1057 (2011).
 - [6] Y. Ando, Topological Insulator Materials, *Journal of the Physical Society of Japan* **82**, 102001 (2013).
 - [7] N. Nagaosa and Y. Tokura, Topological properties and dynamics of magnetic skyrmions, *Nature Nanotechnology* **8**, 899 (2013).
 - [8] Y. Fujishiro, N. Kanazawa, and Y. Tokura, Engineering skyrmions and emergent monopoles in topological spin crystals, *Applied Physics Letters* **116**, 090501 (2020).
 - [9] A. Kitaev, Anyons in an exactly solved model and beyond, *Annals of Physics* **321**, 2 (2006).
 - [10] S. Trebst and C. Hickey, Kitaev materials, *Physics Reports* **950**, 1 (2022).
 - [11] M. Hermanns, I. Kimchi, and J. Knolle, Physics of the Kitaev Model: Fractionalization, Dynamic Correlations, and Material Connections, *Annual Review of Condensed Matter Physics* **9**, 17 (2018).
 - [12] Y. Motome and J. Nasu, Hunting majorana fermions in kitaev magnets, *Journal of the Physical Society of Japan* **89**, 012002 (2020).
 - [13] H. Takagi, T. Takayama, G. Jackeli, G. Khaliullin, and S. E. Nagler, Concept and realization of Kitaev quantum spin liquids, *Nature Reviews Physics* **1**, 264 (2019).
 - [14] L. Janssen and M. Vojta, Heisenberg–Kitaev physics in magnetic fields, *Journal of Physics: Condensed Matter* **31**, 423002 (2019).
 - [15] Y. Motome, R. Sano, S. Jang, Y. Sugita, and Y. Kato, Materials design of kitaev spin liquids beyond the jackeli–khaliullin mechanism, *Journal of Physics: Condensed Matter* **32**, 404001 (2020).
 - [16] L. Zhang and Y. Motome, Possible Realization of Kitaev Spin Liquids in van der Waals Heterostructures of α -RuCl₃ and CrX₃ (X=Cl and I), arXiv preprint arXiv:2310.01075 (2023).

- [17] I. Dzyaloshinsky, A thermodynamic theory of “weak” ferromagnetism of antiferromagnetics, *Journal of Physics and Chemistry of Solids* **4**, 241 (1958).
- [18] T. Moriya, Anisotropic Superexchange Interaction and Weak Ferromagnetism, *Phys. Rev.* **120**, 91 (1960).
- [19] S. Mühlbauer, B. Binz, F. Jonietz, C. Pfleiderer, A. Rosch, A. Neubauer, R. Georgii, and P. Boni, Skyrmion Lattice in a Chiral Magnet, *Science* **323**, 915 (2009).
- [20] X. Z. Yu, Y. Onose, N. Kanazawa, J. H. Park, J. H. Han, Y. Matsui, N. Nagaosa, and Y. Tokura, Real-space observation of a two-dimensional skyrmion crystal, *Nature* **465**, 901 (2010).
- [21] S. Seki, X. Z. Yu, S. Ishiwata, and Y. Tokura, Observation of Skyrmions in a Multiferroic Material, *Science* **336**, 198 (2012).
- [22] I. Kézsmárki, S. Bordács, P. Milde, E. Neuber, L. M. Eng, J. S. White, H. M. Rønnow, C. D. Dewhurst, M. Mochizuki, K. Yanai, H. Nakamura, D. Ehlers, V. Tsurkan, and A. Loidl, Néel-type skyrmion lattice with confined orientation in the polar magnetic semiconductor GaV₄S₈, *Nature Materials* **14**, 1116 (2015).
- [23] T. Kurumaji, T. Nakajima, V. Ukleev, A. Feoktystov, T.-h. Arima, K. Kakurai, and Y. Tokura, Néel-Type Skyrmion Lattice in the Tetragonal Polar Magnet VOSe₂O₅, *Phys. Rev. Lett.* **119**, 237201 (2017).
- [24] Y. Togawa, T. Koyama, K. Takayanagi, S. Mori, Y. Kousaka, J. Akimitsu, S. Nishihara, K. Inoue, A. S. Ovchinnikov, and J. Kishine, Chiral Magnetic Soliton Lattice on a Chiral Helimagnet, *Phys. Rev. Lett.* **108**, 107202 (2012).
- [25] J. ichiro Kishine and A. Ovchinnikov, Theory of Monoaxial Chiral Helimagnet, in *Solid State Physics* (Elsevier, 2015) pp. 1–130.
- [26] Y. Togawa, Y. Kousaka, K. Inoue, and J. ichiro Kishine, Symmetry, Structure, and Dynamics of Monoaxial Chiral Magnets, *Journal of the Physical Society of Japan* **85**, 112001 (2016).
- [27] N. Kanazawa, Y. Onose, T. Arima, D. Okuyama, K. Ohoyama, S. Wakimoto, K. Kakurai, S. Ishiwata, and Y. Tokura, Large Topological Hall Effect in a Short-Period Helimagnet MnGe, *Phys. Rev. Lett.* **106**, 156603 (2011).
- [28] T. Tanigaki, K. Shibata, N. Kanazawa, X. Yu, Y. Onose, H. S. Park, D. Shindo, and Y. Tokura, Real-Space Observation of Short-Period Cubic Lattice of Skyrmions in MnGe, *Nano Letters* **15**, 5438 (2015).
- [29] N. Kanazawa, Y. Nii, X. X. Zhang, A. S. Mishchenko, G. D. Filippis, F. Kagawa, Y. Iwasa, N. Nagaosa, and Y. Tokura, Critical phenomena of emergent magnetic monopoles in a chiral magnet, *Nature Communications* **7**, 11622 (2016).
- [30] Y. Fujishiro, N. Kanazawa, T. Nakajima, X. Z. Yu, K. Ohishi, Y. Kawamura, K. Kakurai, T. Arima, H. Mitamura, A. Miyake, K. Akiba, M. Tokunaga, A. Matsuo, K. Kindo, T. Koretsune, R. Arita, and Y. Tokura, Topological transitions among skyrmion- and hedgehog-lattice states in cubic chiral magnets, *Nature Communications* **10**, 1059 (2019).
- [31] N. Nagaosa and Y. Tokura, Emergent electromagnetism in solids, *Physica Scripta* **T146**, 014020 (2012).
- [32] M. Mochizuki, Spin-Wave Modes and Their Intense Excitation Effects in Skyrmion Crystals, *Phys. Rev. Lett.* **108**, 017601 (2012).
- [33] S. Seki and M. Mochizuki, *Skyrmions in magnetic materials* (Springer, 2016).
- [34] A. Kitaev, Anyons in an exactly solved model and beyond, *Annals of Physics* **321**, 2 (2006).
- [35] G. Baskaran, S. Mandal, and R. Shankar, Exact Results for Spin Dynamics and Fractionalization in the Kitaev Model, *Phys. Rev. Lett.* **98**, 247201 (2007).
- [36] G. Jackeli and G. Khaliullin, Mott Insulators in the Strong Spin-Orbit Coupling Limit: From Heisenberg to a Quantum Compass and Kitaev Models, *Phys. Rev. Lett.* **102**, 017205 (2009).
- [37] J. Knolle, D. L. Kovrizhin, J. T. Chalker, and R. Moessner, Dynamics of a Two-Dimensional Quantum Spin Liquid: Signatures of Emergent Majorana Fermions and Fluxes, *Phys. Rev. Lett.* **112**, 207203 (2014).
- [38] Y. Yamaji, Y. Nomura, M. Kurita, R. Arita, and M. Imada, First-Principles Study of the Honeycomb-Lattice Iridates Na₂IrO₃ in the Presence of Strong Spin-Orbit Interaction and Electron Correlations, *Phys. Rev. Lett.* **113**, 107201 (2014).
- [39] J. Nasu, M. Udagawa, and Y. Motome, Thermal fractionalization of quantum spins in a Kitaev model: Temperature-linear specific heat and coherent transport of Majorana fermions, *Phys. Rev. B* **92**, 115122 (2015).
- [40] K. O’Brien, M. Hermanns, and S. Trebst, Classification of gapless F_2 spin liquids in three-dimensional kitaev models, *Phys. Rev. B* **93**, 085101 (2016).
- [41] A. Bolens, H. Katsura, M. Ogata, and S. Miyashita, Mechanism for subgap optical conductivity in honeycomb kitaev materials, *Phys. Rev. B* **97**, 161108 (2018).
- [42] N. Romming, C. Hanneken, M. Menzel, J. E. Bickel, B. Wolter, K. von Bergmann, A. Kubetzka, and R. Wiesendanger, Writing and Deleting Single Magnetic Skyrmions, *Science* **341**, 636 (2013).
- [43] P.-J. Hsu, A. Kubetzka, A. Finco, N. Romming, K. von Bergmann, and R. Wiesendanger, Electric-field-driven switching of individual magnetic skyrmions, *Nature Nanotechnology* **12**, 123 (2016).
- [44] J. Matsuno, N. Ogawa, K. Yasuda, F. Kagawa, W. Koshibae, N. Nagaosa, Y. Tokura, and M. Kawasaki, Interface-driven topological hall effect in SrRuO₃-SrIrO₃ bilayer, *Science Advances* **2**, e1600304 (2016).
- [45] S. I. Vishkayi, Z. Torbatian, A. Qaiumzadeh, and R. Asgari, Strain and electric-field control of spin-spin interactions in monolayer crI₃, *Phys. Rev. Materials* **4**, 094004 (2020).
- [46] C.-K. Li, X.-P. Yao, and G. Chen, Writing and deleting skyrmions with electric fields in a multiferroic heterostructure, *Phys. Rev. Research* **3**, L012026 (2021).
- [47] M. Kanega, T. N. Ikeda, and M. Sato, Linear and nonlinear optical responses in kitaev spin liquids, *Phys. Rev. Research* **3**, L032024 (2021).
- [48] Y. Zhang, J. Liu, Y. Dong, S. Wu, J. Zhang, J. Wang, J. Lu, A. Rückriegel, H. Wang, R. Duine, H. Yu, Z. Luo, K. Shen, and J. Zhang, Strain-driven dzyaloshinskii-moriya interaction for room-temperature magnetic skyrmions, *Phys. Rev. Lett.* **127**, 117204 (2021).
- [49] Y. Tokura, S. Seki, and N. Nagaosa, Multiferroics of spin origin, *Reports on Progress in Physics* **77**, 076501 (2014).
- [50] F. Matsukura, Y. Tokura, and H. Ohno, Control of magnetism by electric fields, *Nature Nanotechnology* **10**, 209 (2015).

- [51] T. Kimura, T. Goto, H. Shintani, K. Ishizaka, T. Arima, and Y. Tokura, Magnetic control of ferroelectric polarization, *Nature* **426**, 55 (2003).
- [52] H. Katsura, N. Nagaosa, and A. V. Balatsky, Spin Current and Magnetoelectric Effect in Noncollinear Magnets, *Phys. Rev. Lett.* **95**, 057205 (2005).
- [53] M. Mostovoy, Ferroelectricity in Spiral Magnets, *Phys. Rev. Lett.* **96**, 067601 (2006).
- [54] I. A. Sergienko and E. Dagotto, Role of the Dzyaloshinskii-Moriya interaction in multiferroic perovskites, *Phys. Rev. B* **73**, 094434 (2006).
- [55] S.-W. Cheong and M. Mostovoy, Multiferroics: a magnetic twist for ferroelectricity, *Nature Materials* **6**, 13 (2007).
- [56] T. Arima, Ferroelectricity Induced by Proper-Screw Type Magnetic Order, *Journal of the Physical Society of Japan* **76**, 073702 (2007).
- [57] M. Mostovoy, K. Nomura, and N. Nagaosa, Theory of electric polarization in multiorbital mott insulators, *Phys. Rev. Lett.* **106**, 047204 (2011).
- [58] S. Z. Bisri, S. Shimizu, M. Nakano, and Y. Iwasa, Endeavor of Iontronics: From Fundamentals to Applications of Ion-Controlled Electronics, *Advanced Materials* **29**, 1607054 (2017).
- [59] K. Ueno, H. Shimotani, H. Yuan, J. Ye, M. Kawasaki, and Y. Iwasa, Field-Induced Superconductivity in Electric Double Layer Transistors, *Journal of the Physical Society of Japan* **83**, 032001 (2014).
- [60] K. Yazawa, D. Drury, A. Zakutayev, and G. L. Brennecke, Reduced coercive field in epitaxial thin film of ferroelectric wurtzite $\text{Al}_0.7\text{Sc}_0.3\text{N}$, *Applied Physics Letters* **118**, 10.1063/5.0043613 (2021).
- [61] T. Mikolajick, S. Slesazek, H. Mulaosmanovic, M. H. Park, S. Fichtner, P. D. Lomenzo, M. Hoffmann, and U. Schroeder, Next generation ferroelectric materials for semiconductor process integration and their applications, *Journal of Applied Physics* **129**, 10.1063/5.0037617 (2021).
- [62] G. Chen, T. Ma, A. T. N'Diaye, H. Kwon, C. Won, Y. Wu, and A. K. Schmid, Tailoring the chirality of magnetic domain walls by interface engineering, *Nature Communications* **4**, 10.1038/ncomms3671 (2013).
- [63] K.-W. Kim, H.-W. Lee, K.-J. Lee, and M. D. Stiles, Chirality from interfacial spin-orbit coupling effects in magnetic bilayers, *Phys. Rev. Lett.* **111**, 216601 (2013).
- [64] C. Huang, L. Z. Jiang, Y. Zhu, Y. F. Pan, J. Y. Fan, C. L. Ma, J. Hu, and D. N. Shi, Tuning dzyaloshinskii-moriya interaction via an electric field at the co/h-bn interface, *Physical Chemistry Chemical Physics* **23**, 22246–22250 (2021).
- [65] J. Chen, *Introduction to Scanning Tunneling Microscopy Third Edition*, Vol. 69 (Oxford University Press, USA, 2021).
- [66] N. P. Magtoto, C. Niu, B. M. Ekstrom, S. Addepalli, and J. A. Kelber, Dielectric breakdown of ultrathin aluminum oxide films induced by scanning tunneling microscopy, *Applied Physics Letters* **77**, 2228 (2000).
- [67] K. Takasan and M. Sato, Control of magnetic and topological orders with a DC electric field, *Phys. Rev. B* **100**, 060408 (2019).
- [68] S. C. Furuya, K. Takasan, and M. Sato, Control of superexchange interactions with DC electric fields, *Phys. Rev. Research* **3**, 033066 (2021).
- [69] P. Noh, K. Hwang, and E.-G. Moon, Manipulating Topological Quantum Phase Transitions of Kitaev's Quantum Spin Liquids with Electric Fields, *arXiv preprint arXiv:2308.00760* (2023).
- [70] G. Khaliullin, Orbital Order and Fluctuations in Mott Insulators, *Progress of Theoretical Physics Supplement* **160**, 155 (2005).
- [71] H. Ohno, D. Chiba, F. Matsukura, T. Omiya, E. Abe, T. Dietl, Y. Ohno, and K. Ohtani, Electric-field control of ferromagnetism, *Nature* **408**, 944 (2000).
- [72] L. Chen, F. Matsukura, and H. Ohno, Electric-Field Modulation of Damping Constant in a Ferromagnetic Semiconductor (Ga,Mn)As, *Phys. Rev. Lett.* **115**, 057204 (2015).
- [73] S. Jiang, J. Shan, and K. F. Mak, Electric-field switching of two-dimensional van der Waals magnets, *Nature Materials* **17**, 406 (2018).
- [74] B. Huang, G. Clark, D. R. Klein, D. MacNeill, E. Navarro-Moratalla, K. L. Seyler, N. Wilson, M. A. McGuire, D. H. Cobden, D. Xiao, W. Yao, P. Jarillo-Herrero, and X. Xu, Electrical control of 2D magnetism in bilayer CrI_3 , *Nature Nanotechnology* **13**, 544 (2018).
- [75] X. Chen, X. Zhou, R. Cheng, C. Song, J. Zhang, Y. Wu, Y. Ba, H. Li, Y. Sun, Y. You, Y. Zhao, and F. Pan, Electric field control of Néel spin-orbit torque in an antiferromagnet, *Nature Materials* **18**, 931 (2019).
- [76] C. Xu, P. Chen, H. Tan, Y. Yang, H. Xiang, and L. Bellaiche, Electric-Field Switching of Magnetic Topological Charge in Type-I Multiferroics, *Phys. Rev. Lett.* **125**, 037203 (2020).
- [77] H. Hirori, A. Doi, F. Blanchard, and K. Tanaka, Single-cycle terahertz pulses with amplitudes exceeding 1 MV/cm generated by optical rectification in LiNbO_3 , *Applied Physics Letters* **98**, 091106 (2011).
- [78] Y. Mukai, H. Hirori, T. Yamamoto, H. Kageyama, and K. Tanaka, Nonlinear magnetization dynamics of antiferromagnetic spin resonance induced by intense terahertz magnetic field, *New Journal of Physics* **18**, 013045 (2016).
- [79] D. Nicoletti and A. Cavalleri, Nonlinear light-matter interaction at terahertz frequencies, *Advances in Optics and Photonics* **8**, 401 (2016).
- [80] J. A. Fülöp, S. Tzortzakis, and T. Kampfrath, Laser-Driven Strong-Field Terahertz Sources, *Advanced Optical Materials* **8**, 1900681 (2019).
- [81] M. Sato, S. Takayoshi, and T. Oka, Laser-Driven Multiferroics and Ultrafast Spin Current Generation, *Phys. Rev. Lett.* **117**, 147202 (2016).
- [82] M. Sato, Floquet theory and ultrafast control of magnetism, Chirality, Magnetism and Magnetoelectricity: Separate Phenomena and Joint Effects in Metamaterial Structures **138**, 265 (2021).
- [83] H. Eskes and J. H. Jefferson, Superexchange in the cuprates, *Phys. Rev. B* **48**, 9788 (1993).
- [84] H. Liu and G. Khaliullin, Pseudospin exchange interactions in d^7 cobalt compounds: Possible realization of the kitaev model, *Phys. Rev. B* **97**, 014407 (2018).
- [85] Y. Sugita, Y. Kato, and Y. Motome, Antiferromagnetic kitaev interactions in polar spin-orbit mott insulators, *Phys. Rev. B* **101**, 100410 (2020).
- [86] S. Sugano, Y. Tanabe, and H. Kamimura, *Multiplets of transition-metal ions in crystals* (Academic Press, New York, 1970).
- [87] B. J. Kim, H. Jin, S. J. Moon, J.-Y. Kim, B.-G. Park, C. S. Leem, J. Yu, T. W. Noh, C. Kim, S.-J. Oh,

- J.-H. Park, V. Durairaj, G. Cao, and E. Rotenberg, Novel $J_{\text{eff}} = 1/2$ Mott State Induced by Relativistic Spin-Orbit Coupling in Sr_2IrO_4 , *Phys. Rev. Lett.* **101**, 076402 (2008).
- [88] Y. Onodera and M. Okazaki, Tables of Basis Functions for Double Point Groups, *Journal of the Physical Society of Japan* **21**, 2400 (1966).
- [89] T. Takayama, J. Chaloupka, A. Smerald, G. Khaliullin, and H. Takagi, Spin-Orbit-Entangled Electronic Phases in 4d and 5d Transition-Metal Compounds, *Journal of the Physical Society of Japan* **90**, 062001 (2021).
- [90] H. Matsuura and K. Miyake, Effect of Spin-Orbit Interaction on (4d)3- and (5d)3-Based Transition-Metal Oxides, *Journal of the Physical Society of Japan* **82**, 073703 (2013).
- [91] H. Matsuura and M. Ogata, A Poor Man's Derivation of Quantum Compass-Heisenberg Interaction: Superexchange Interaction in J-J Coupling Scheme, *Journal of the Physical Society of Japan* **83**, 093701 (2014).
- [92] J. B. Goodenough, Theory of the Role of Covalence in the Perovskite-Type Manganites $[\text{La}, M(\text{II})]\text{MnO}_3$, *Phys. Rev.* **100**, 564 (1955).
- [93] J. Kanamori, Theory of the Magnetic Properties of Ferrous and Cobaltous Oxides, I, *Progress of Theoretical Physics* **17**, 177 (1957).
- [94] J. Kanamori, Theory of the Magnetic Properties of Ferrous and Cobaltous Oxides, II, *Progress of Theoretical Physics* **17**, 197 (1957).
- [95] C. Xu, J. Feng, H. Xiang, and L. Bellaiche, Interplay between kitaev interaction and single ion anisotropy in ferromagnetic CrI_3 and CrGeTe_3 monolayers, *npj Computational Materials* **4**, 57 (2018).
- [96] P. P. Stavropoulos, D. Pereira, and H.-Y. Kee, Microscopic mechanism for a higher-spin kitaev model, *Phys. Rev. Lett.* **123**, 037203 (2019).
- [97] D. Takikawa and S. Fujimoto, Impact of off-diagonal exchange interactions on the kitaev spin-liquid state of $\alpha\text{-RuCl}_3$, *Phys. Rev. B* **99**, 224409 (2019).
- [98] D. Takikawa and S. Fujimoto, Topological phase transition to abelian anyon phases due to off-diagonal exchange interaction in the kitaev spin liquid state, *Phys. Rev. B* **102**, 174414 (2020).
- [99] A. Banerjee, C. A. Bridges, J.-Q. Yan, A. A. Aczel, L. Li, M. B. Stone, G. E. Granroth, M. D. Lumsden, Y. Yiu, J. Knolle, S. Bhattacharjee, D. L. Kovrizhin, R. Moessner, D. A. Tennant, D. G. Mandrus, and S. E. Nagler, Proximate Kitaev quantum spin liquid behaviour in a honeycomb magnet, *Nature Materials* **15**, 733 (2016).
- [100] R. Yadav, N. A. Bogdanov, V. M. Katukuri, S. Nishimoto, J. van den Brink, and L. Hozoi, Kitaev exchange and field-induced quantum spin-liquid states in honeycomb $\alpha\text{-RuCl}_3$, *Scientific Reports* **6**, 10.1038/srep37925 (2016).
- [101] A. Glamazda, P. Lemmens, S.-H. Do, Y. S. Kwon, and K.-Y. Choi, Relation between Kitaev magnetism and structure in $\alpha\text{-RuCl}_3$, *Phys. Rev. B* **95**, 174429 (2017).
- [102] A. U. B. Wolter, L. T. Corredor, L. Janssen, K. Nenkov, S. Schönecker, S.-H. Do, K.-Y. Choi, R. Albrecht, J. Hunger, T. Doert, M. Vojta, and B. Büchner, Field-induced quantum criticality in the Kitaev system $\alpha\text{-RuCl}_3$, *Phys. Rev. B* **96**, 041405 (2017).
- [103] Y. Kasahara, K. Sugii, T. Ohnishi, M. Shimozawa, M. Yamashita, N. Kurita, H. Tanaka, J. Nasu, Y. Motome, T. Shibauchi, and Y. Matsuda, Unusual Thermal Hall Effect in a Kitaev Spin Liquid Candidate $\alpha\text{-RuCl}_3$, *Phys. Rev. Lett.* **120**, 217205 (2018).
- [104] D. Wulferding, Y. Choi, S.-H. Do, C. H. Lee, P. Lemmens, C. Faugeras, Y. Gallais, and K.-Y. Choi, Magnon bound states versus anyonic Majorana excitations in the Kitaev honeycomb magnet $\alpha\text{-RuCl}_3$, *Nature Communications* **11**, 10.1038/s41467-020-15370-1 (2020).
- [105] M. Yamashita, J. Gouchi, Y. Uwatoko, N. Kurita, and H. Tanaka, Sample dependence of half-integer quantized thermal hall effect in the kitaev spin-liquid candidate $\alpha\text{-RuCl}_3$, *Phys. Rev. B* **102**, 220404 (2020).
- [106] H. Suzuki, H. Liu, J. Bertinshaw, K. Ueda, H. Kim, S. Laha, D. Weber, Z. Yang, L. Wang, H. Takahashi, K. Fürsich, M. Minola, B. V. Lotsch, B. J. Kim, H. Yavaş, M. Daghofer, J. Chaloupka, G. Khaliullin, H. Gretarsson, and B. Keimer, Proximate ferromagnetic state in the Kitaev model material $\alpha\text{-RuCl}_3$, *Nature Communications* **12**, 4512 (2021).
- [107] A. Ralko and J. Merino, Novel chiral quantum spin liquids in kitaev magnets, *Phys. Rev. Lett.* **124**, 217203 (2020).
- [108] H. Min, J. E. Hill, N. A. Sinitsyn, B. R. Sahu, L. Kleinman, and A. H. MacDonald, Intrinsic and Rashba spin-orbit interactions in graphene sheets, *Phys. Rev. B* **74**, 165310 (2006).
- [109] A. D. Caviglia, M. Gabay, S. Gariglio, N. Reyren, C. Cancellieri, and J.-M. Triscone, Tunable Rashba Spin-Orbit Interaction at Oxide Interfaces, *Phys. Rev. Lett.* **104**, 126803 (2010).
- [110] C. R. Ast, J. Henk, A. Ernst, L. Moreschini, M. C. Falub, D. Pacilé, P. Bruno, K. Kern, and M. Gioni, Giant spin splitting through surface alloying, *Phys. Rev. Lett.* **98**, 186807 (2007).
- [111] K. V. Shanavas and S. Satpathy, Electric field tuning of the rashba effect in the polar perovskite structures, *Phys. Rev. Lett.* **112**, 086802 (2014).
- [112] K. Shimizu, S. Okumura, Y. Kato, and Y. Motome, Spin moiré engineering of topological magnetism and emergent electromagnetic fields, *Phys. Rev. B* **103**, 184421 (2021).
- [113] C. J. Chen, *Introduction to Scanning Tunneling Microscopy* (Oxford University Press/Oxford, 2007).
- [114] A. Kirilyuk, A. V. Kimel, and T. Rasing, Ultrafast optical manipulation of magnetic order, *Rev. Mod. Phys.* **82**, 2731 (2010).
- [115] T. Nakagawara, M. Kanega, S. C. Furuya, and M. Sato, In preparation.
- [116] G. Yu, P. Upadhyaya, X. Li, W. Li, S. K. Kim, Y. Fan, K. L. Wong, Y. Tserkovnyak, P. K. Amiri, and K. L. Wang, Room-temperature creation and spin-orbit torque manipulation of skyrmions in thin films with engineered asymmetry, *Nano Letters* **16**, 1981–1988 (2016).
- [117] T. Srivastava, M. Schott, R. Juge, V. Křížáková, M. Belmeguenai, Y. Roussigné, A. Bernard-Mantel, L. Ranno, S. Pizzini, S.-M. Chérif, A. Stashkevich, S. Auffret, O. Boulle, G. Gaudin, M. Chshiev, C. Baraduc, and H. Béa, Large-voltage tuning of dzyaloshinskii-moriya interactions: A route toward dynamic control of skyrmion chirality, *Nano Letters* **18**, 4871–4877 (2018).
- [118] K. W. Plumb, J. P. Clancy, L. J. Sandilands, V. V. Shankar, Y. F. Hu, K. S. Burch, H.-Y. Kee, and Y.-J.

- Kim, α - rUCl_3 : A spin-orbit assisted mott insulator on a honeycomb lattice, *Phys. Rev. B* **90**, 041112 (2014).
- [119] K. S. Burch, D. Mandrus, and J.-G. Park, Magnetism in two-dimensional van der waals materials, *Nature* **563**, 47–52 (2018).
- [120] N. Mounet, M. Gibertini, P. Schwaller, D. Campi, A. Merkys, A. Marrazzo, T. Sohier, I. E. Castelli, A. Cepellotti, G. Pizzi, and N. Marzari, Two-dimensional materials from high-throughput computational exfoliation of experimentally known compounds, *Nature Nanotechnology* **13**, 246–252 (2018).
- [121] S. Jiang, J. Shan, and K. F. Mak, Electric-field switching of two-dimensional van der waals magnets, *Nature Materials* **17**, 406 (2018).
- [122] B. Huang, G. Clark, D. R. Klein, D. MacNeill, E. Navarro-Moratalla, K. L. Seyler, N. Wilson, M. A. McGuire, D. H. Cobden, D. Xiao, W. Yao, P. Jarillo-Herrero, and X. Xu, Electrical control of 2d magnetism in bilayer CrI_3 , *Nature Nanotechnology* **13**, 544 (2018).